https://doi.org/10.5194/egusphere-2026-1939
Preprint. Discussion started: 10 April 2026
© Author(s) 2026. CC BY 4.0 License.

Temporal variation of northern midlatitude baseline ozone: 48-year observational record challenges our understanding of tropospheric chemistry

David D. Parrish[1], Charles A. Mims[2], Richard G. Derwent[3], Ian C. Faloona[4,5], Henry Bowman[6], Tongwen Wu[7], Jie Zhang[7], Makoto Deushi[8], Naga Oshima[8]

[1] David.D.Parrish, LLC, 4630 MacArthur Ln, Boulder, Colorado, USA
[2] Department of Chemical Engineering & Applied Chemistry, University of Toronto Ontario, Canada.
[3] rdscientific, Newbury, Berkshire, UK
[4] Air Quality Research Center, University of CA, Davis, CA, USA
[5] Department of Land, Air, & Water Resources, University of CA, Davis, CA, USA
[6] School of Engineering & Applied Sciences, Harvard University, Cambridge, Massachusetts 02138, USA
[7] Beijing Climate Center, China Meteorological Administration, Beijing, China
[8] Meteorological Research Institute, 1-1 Nagamine, Tsukuba, Ibaraki, 305-0052, Japan

Correspondence to: David D. Parrish (david.d.parrish.llc@gmail.com)

Abstract. A continuous, 48-year measurement record, plus some earlier measurements, of baseline ozone at northern mid-latitudes are analyzed to quantify seasonal cycles and long-term changes of annual mean tropospheric ozone. Long-term changes are similar at all sites, and seasonal cycles are similar in the marine boundary layer (MBL) and in the free troposphere (FT), but with marked differences between those two environments. Over the last half of the 20th century, ozone concentrations increased by a factor of ~2, the seasonal cycle amplitude increased by nearly 50%, and its maximum shifted to later in the year by 10 ± 13 days. The long-term increase ended early in the 21st century, followed by a slow decrease that reversed only a small fraction of the total earlier increase. In contrast, the seasonal cycle returned to near that of the preindustrial period. Simulations by six earth system models agree with the magnitude of the overall ozone increase and the increase ending early this century; however, observations indicate only a post-1950 increase, while models simulate a slower increase beginning in 1850. Consequently, the high bias of model simulations, while modest (~10%) in recent years, was much larger (~87%) in the 1950s. Qualitatively similar seasonal cycles and shifts are seen in the measurements and simulations, but simulations do not show the observed strong separation between MBL and FT behavior. We hypothesize that models simulate a background troposphere that is too NOx-rich, implying a lesser role than models simulate for methane in raising background ozone concentrations.

https://doi.org/10.5194/egusphere-2026-1939
Preprint. Discussion started: 10 April 2026
© Author(s) 2026. CC BY 4.0 License.

1 Introduction

Ozone is one of the most important trace species of the troposphere. It is both an air pollutant, damaging to human health and ecosystems, and a greenhouse gas, contributing to climate warming. It is also the dominant precursor of hydroxyl radicals, which in turn drive the photochemical processes that remove many pollutants from the atmosphere and determine the concentration of trace species in the troposphere. These processes can also produce ozone during oxidation of precursor species emitted from both anthropogenic and natural sources. Quantifying the spatial distribution of ozone and its temporal variability on seasonal and long-term (i.e., decadal scale) time scales is critical to our understanding of tropospheric composition and climate change. The first goal of this paper is to improve that quantification within the background troposphere at northern midlatitudes through analysis of the available 48-year record of ozone observations. Here we use the term "baseline" to refer to air masses that have not recently (i.e., on a synoptic scale of about 3-20 days) been influenced by continental ozone sources or sinks; it is these air masses that represent the background troposphere. Ozone precursor emissions are predominately localized in the continental boundary layer, resulting in significantly more complex temporal ozone variability there than in the background troposphere; we will not consider this more complex regime. Northern mid-latitudes is a zone of particular interest because anthropogenic ozone precursors were predominantly emitted here during the early decades of industrial development, and those emissions have decreased over more recent decades. Moreover, our analysis is observationally-based, and the historical record of ozone measurements is most extensive in this region. The second goal of this paper is to present the derived quantification of ozone variability in a coherent context so as to enhance our conceptual understanding of the ozone sources and sinks that drives this variability. Essential to that presentation is a comparison of the observational analysis results with global model simulations of the zonal tropospheric ozone distribution.

Global model simulations find that the mean lifetime of ozone in the troposphere is on the order of 3 weeks (e.g., Stevenson et al., 2006; Young et al., 2013). However, ozone loss is relatively fast in the tropics and the moist planetary boundary layer, so the local and regional ozone lifetime is heterogenous, with a mean net lifetime in an isolated, free troposphere (FT) air parcel at northern midlatitudes of several months or longer (see detailed discussion in Parrish et al., 2021a). The mean zonal wind speed in the FT provides a circum-global transport time that is shorter than this mean net ozone lifetime; therefore, mean ozone concentrations exhibit a significant degree of zonal homogeneity in the northern midlatitude FT. Parrish et al. (2020) examined this homogeneity, and found similar long-term changes and mean seasonal cycles throughout the FT, albeit with a significant positive vertical gradient driven by the separation between the important ozone source from the stratosphere and the prevailing boundary-layer ozone loss (photochemistry in pristine marine environments and/or dry deposition onto continental vegetation). Since entrainment of ozone from the FT is the predominant source of ozone to the marine boundary layer (MBL), long-term ozone changes in this layer are similar to those in the FT. However, the MBL exhibits a very different ozone seasonal cycle from that in the FT due to the large seasonal variation of ozone loss in the MBL. Mims et al. (2022) present a conceptual model of baseline ozone at northern midlatitudes, one that quantitatively captures many of the primary features of the baseline ozone distribution in the troposphere, including the

https://doi.org/10.5194/egusphere-2026-1939
Preprint. Discussion started: 10 April 2026
© Author(s) 2026. CC BY 4.0 License.

stronger vertical gradients over maritime regions and the phase delay in the FT seasonal cycle from the peak injection time of stratosphere-to-troposphere exchange.

The large degree of zonal similarity ensures that analysis of only a relatively few data sets is required to provide a comprehensive quantification. Parrish et al. (2020) analyzed eight high quality, in situ measurement data sets from baseline representative sites with the longest records in order to quantify baseline ozone changes from 1978, the beginning of the earliest measurement record, through 2018. These sites are near the western coasts of Europe and North America, include MBL and FT surface sites as well as data from balloon-borne sondes and commercial aircraft. This paper extends that analysis to include up to 9 additional years of measurements in those records available by late 2025, and also includes additional analyses. Specific issues we address include 1) more accurate and precise quantification of the long-term ozone changes over the longer data records, 2) determination if baseline ozone continues to decrease after a maximum reached in the first decade of this century, since a continuing decrease would bring both climate and air quality benefits, 3) accurate and precise quantification of the change in baseline ozone concentrations during the period of decreased anthropogenic precursor emissions associated with the COVID-19 pandemic, 4) determination of systematic shifts in the phase and amplitude of the baseline ozone seasonal cycle, and 5) comparison of the observational analysis with similar analysis of ozone simulations from global models. In general we attribute the ozone changes to long-term precursor emission changes, so we include some analysis of cause and effect mechanisms.

2 Data and analysis methods

2.1 Data sets analyzed

The eight baseline representative data sets analyzed by Parrish et al. (2020), with the additional measurement data now available, are analyzed in this work. That earlier paper gives descriptions of each data set and includes site locations and elevations in their Table 1. To improve signal to noise in the analysis of long-term ozone changes in this work, each pair of FT data sets over Europe and North America are combined into a single FT data set over the respective continents. Tables S1 and S2 of the Supplement give the total time spans and numbers of monthly means of the extended data sets analyzed here.

Some specific details of the extended data sets analyzed here should be noted:

- Mace Head data are the monthly mean baseline ozone mixing ratios analyzed by Derwent et al. (2024). These have been filtered by meteorological analyses to select ozone data that are representative of the unpolluted Northern Hemispheric marine boundary layer. They span April 1987 – May 2022 and are available from Appendix A of that reference.
- The Pacific MBL data set was collected at four measurement sites along the northern US Pacific Coast beginning in November 1987. This record is here extended through the end of 2024 with monthly means calculated from Trinidad Head surface site hourly data downloaded from the NOAA Global Monitoring Laboratory data archive (https://gml.noaa.gov/ozwv/surfoz/, last accessed 11 November 2025). These Trinidad Head surface ozone data are described by Effertz, Peter; Petropavlovskikh, Irina (2026). NOAA Earth System Research Laboratory Surface Ozone

https://doi.org/10.5194/egusphere-2026-1939
Preprint. Discussion started: 10 April 2026
© Author(s) 2026. CC BY 4.0 License.

Data, Version 2 from 1973-09-13 to 2024-12-31 (NCEI Accession 0312023). NOAA National Centers for Environmental Information. Dataset. https://doi.org/10.25921/hbbh-0q04. Version 1 of the data were accessed through 2023 and Version 2 for 2024. No data were reported for 22 months (July-December, 2017 and October 2018-December 2019) during the 2017-2019 period, or for March-July 2023. In previous analyses, relatively high speed, on-shore wind periods were selected to isolate baseline representative data (Parrish et al., 2009) for all months through May 2017; however, recent wind data are not available at the Trinidad Head Observatory, so baseline ozone concentrations for later months are estimated from the full ozone data set as described in Section S1 of the Supplement. The monthly and annual means for this complete data set, along with the identity and measurement periods of the four sites, are given in Table S7 of the Supplement.

- The Lassen NP data set is collected at an elevated, inland site in northern California; here it is extended with monthly means calculated from hourly data available from the U.S. National Park Service (https://ard-request.air-resource.com/data.aspx, last accessed 7 November 2025). With the exception of August 2025, all monthly means over the 38 years of measurements from October 1987 through September 2025 are available and included in the analysis.
- The European alpine data set comprises monthly means calculated from measurements at three surface sites in the European Alps; here it is extended with monthly means calculated from hourly data available from the EBAS database (https://ebas.nilu.no/data-access/, last accessed 22 November 2025) operated by the Norwegian Institute for Air Research (NILU). The German Environment Agency provided the Zugspitze-Schneefernerhaus surface ozone data, which began in January 1978; Trikl et al. (2023) present a recent analysis of this data set. Measurements at the Jungfraujoch site began in January 1990 and are now part of the Swiss National Air Pollution Monitoring Network operated jointly by EMPA and the Swiss Federal Office for the Environment. The Environment Agency Austria provided the ozone data from the Sonnblick site, which also began in January 1990. As discussed by Parrish et al. (2020), the Zugspitze data have been collected at two different sites; in later years data from the site at a slightly lower elevation averaged 97.4% of those from the original site so the more recent data are corrected for this difference. A few monthly means are missing from each data set, but averages over the three sites provide an unbroken record of monthly mean ozone over 47 years (1978-2024). The monthly and annual means for this complete data set is given in Table S8 of the Supplement.
- The European sonde data set represents monthly mean data calculated from all sondes launched from three western European sites. In this work the entire data set is recalculated from all sonde files available beginning in 1998 from the Network for the Detection of Atmospheric Composition Change (NDACC) website (www.ndacc.org, last accessed 25 November 2025). In some cases there are minor differences between these files and those analyzed by Parrish et al. (2020). The Hohenpeissenberg data were provided by Wolfgang Steinbrecht of Deutscher Wetterdienst, the Payerne data by Eliane Maillard Barras and Yann Salvi of MeteoSwiss, and the Uccle data by Roeland Van Malderen of the Royal Meteorological Institute of Belgium; Van Malderen et al. (2021) describe a recent analysis of this last data set. Together the three data sets provide a complete record of monthly mean ozone over nearly 28 years (January 1988 –

https://doi.org/10.5194/egusphere-2026-1939
Preprint. Discussion started: 10 April 2026
© Author(s) 2026. CC BY 4.0 License.

October 2025) obtained from a total of. 11,511 sondes. The monthly and annual mean ozone concentrations averaged over the 3 to 9 km altitude range for this complete data set are given in Table S9 of the Supplement.

- IAGOS monthly means are calculated from the 15,915 profiles measured over Frankfurt Germany from August 1994 through September 2023, the latest data posted to the public archive (http://www.iagos.org, last accessed 6 November 2025). The numbers of profiles in several months were limited in the time intervals between the MOZAIC and IAGOS programs, and during the reduced air travel period of the COVID-19 pandemic; months with 4 or fewer profiles are excluded from analysis. This data set was referred to as MOZAIC by Parrish et al. (2020). MOZAIC/CARIBIC/IAGOS data were created with support from the European Commission, national agencies in Germany (BMBF), France (MESR), and the UK (NERC), and the IAGOS member institutions (http://www.iagos.org/partners). The participating airlines (Lufthansa, Air France, Austrian, China Airlines, Hawaiian Airlines, Air Canada, Iberia, Eurowings Discover, Cathay Pacific, Air Namibia, Sabena) supported IAGOS by carrying the measurement equipment free of charge since 1994. The data are available at http://www.iagos.fr thanks to additional support from AERIS.
- The North American free troposphere data are from sondes launched from two sites by the NOAA Global Monitoring Laboratory: Boulder, Colorado beginning in January 1992 and Trinidad Head, California beginning in August 1997. Data downloaded from the laboratory data archive (https://gml.noaa.gov/ozwv/ozsondes/, last accessed 8 November 2025) extended the Boulder data set through September 2025 from a total of 1796 sondes and the Trinidad Head data set through July 2024 from a total of 1657 sondes. The Boulder data provide a complete record of monthly mean ozone over nearly 34 years with an average of 4 to 5 sondes per month.

2.2 Mathematical description and analysis of long-term changes and seasonal cycles

Here we outline our analysis approach and methods; Section S3 of the Supplement gives this same description with additional details discussed. We simultaneously quantify the long-term changes and seasonal cycle of baseline ozone through a least-squares fit of ozone monthly means to Equation 1,

$$O_3(t) = a + bt + ct^2 + dt^3 + A_1*\sin(\chi + \phi_1) + A_2*\sin(2\chi + \phi_2), \quad (1)$$

where t is time in years relative to the year 2000 (i.e., t = year-2000). The seasonal cycle variable, χ, spans one year's time period in radians from 0 to 2π, i.e., $\chi = 2\pi t$, beginning from zero at the start of each year.

The first four terms of Equation 1 are a cubic polynomial that quantifies long-term changes. Cubic polynomial fits to monthly mean ozone concentrations in individual data sets are illustrated in Figs. S1-S4. The parameter values derived in fits of that equation allow calculation of the year that maximum ozone was reached,

$$year_{max} = [-c \pm (c^2 - 3bd)^{1/2}]/3d + 2000; \quad (2)$$

if a quadratic polynomial provides an adequate fit, a simpler equation suffices,

$$year_{max} = -b/2c + 2000. \quad (3)$$

https://doi.org/10.5194/egusphere-2026-1939
Preprint. Discussion started: 10 April 2026
© Author(s) 2026. CC BY 4.0 License.

The final two terms of Equation 1 are the first two terms of a Fourier series: the fundamental (i.e., a single sine cycle per year) and the second harmonic (i.e., two sine cycles per year). Only one or two harmonic terms are generally statistically justified in the fits in this work.

Model simulations have indicated that the seasonal cycle of baseline ozone at northern midlatitudes shifted over past decades, both in magnitude and phase (e.g., Bowman et al., 2022). This shift is attributed to changing anthropogenic precursor emissions; it was initiated by the emission increase that accompanied industrial development, reached a maximum in the late 20th Century, and has since begun to reverse as those emissions have been reduced (Bowman et al., 2022). Fits of Equation (1) quantify the average seasonal cycle over the time period spanned by the fitted data. However, in favorable cases Bowman et al. (2022) find that inclusion of two Gaussian functions can separately describe the shifts in the magnitude and phase of the fundamental of the seasonal cycle; these are added to the A_1 and ϕ_1 parameters in Equation 1:

$$A_1 = A_1^0 + r*\exp\{-((t-m)/s)^2\}, \quad (4)$$

$$\phi_1 = \phi_1^0 + r_\phi*\exp\{-((t-m_\phi)/s_\phi)^2\}. \quad (5)$$

Equations 4 and 5 quantify the shift in the amplitude and phase of the seasonal cycle, respectively. The r and r_ϕ parameters define the magnitude of the Gaussian functions (i.e., the maxima of the shifts in ppb and radians, respectively), the m and m_ϕ parameters give the times (in years relative to the reference year 2000) that those maxima were reached, and the s and s_ϕ parameters quantify the widths in years of the functions. In these equations, the A_1^0 and ϕ_1^0 parameters characterize the amplitude and phase of the preindustrial seasonal cycle, since the Gaussian terms contribute negligibly before ~1900.

Most of the analyses in this work are based upon fits of Equation 1 to the data sets summarized in Section 2.1. In Section 3.4, we investigate long-term shifts in the baseline ozone seasonal cycle for one data set; for this analysis, Equations 4 and 5 are substituted into Equation 1 to derive the fitting equation:

$$O_3(t) = a + bt + ct^2 + dt^3 + (A_1^0 + r*\exp\{-((t-m)/s)^2\})*\sin(\chi + \phi_1^0 + r_\phi*\exp\{-((t- m_\phi)/s_\phi)^2\}) + A_2*\sin(2\chi + \phi_2). \quad (6)$$

The fit of Equation 6 to only one of the ozone data sets gave statistically significant values for the parameters of the Gaussian functions. This particular fit to Equation 6 gave statistically significant values for 12 of the 14 parameters, but the second harmonic did not make a significant contribution. Further, $m_\phi = m$ and $s_\phi = s$ within the derived confidence limits; this equivalence is expected if the shifts in the magnitude and phase of the fundamental arise from the same physical cause, such as changing anthropogenic emissions. Accordingly, the final analysis of this data set is simplified by reducing Equation 6 to Equation 7 with 10 parameter values:

$$O_3(t) = a + bt + ct^2 + dt^3 + (A_1^0 + r*\exp\{-((t-m)/s)^2\})*\sin(\chi + \phi_1^0 + r_\phi*\exp\{-((t-m)/s)^2\}). \quad (7)$$

Unless indicated otherwise, 95% confidence limits are given for the parameter value values; these are calculated from the fits of equations to monthly mean data with corrections for autocorrelation of those means. Section S3.2 of the Supplement discusses these statistical issues in more detail.

https://doi.org/10.5194/egusphere-2026-1939
Preprint. Discussion started: 10 April 2026
© Author(s) 2026. CC BY 4.0 License.

3 Results

3.1 Long-term changes in mean baseline ozone

The time series of monthly mean ozone concentrations from the eight data sets are illustrated together in Fig. 1, and shown more clearly for individual data sets in Figs. S1-S4. These figures include the estimated long-term ozone changes given by fits of Equation 1 to the monthly means and include the derived polynomial coefficient values; Table S1 and S2 collect all derived parameter values, and include additional information. Parrish et al. (2020) fit the earlier years of the same eight data sets (i.e., up to 2014 to 2018, depending upon the data set) with a quadratic, rather than the cubic polynomial utilized here; their Fig. 9 is in the same general format as Fig. 1 to facilitate comparisons, and their Figs. S1-S4 are similarly organized to those same numbered figures in this work. The same general shapes are seen in the fitted curves between the two analyses; however, with the later years of data the coefficients of the cubic terms derived in this work are positive and larger than those derived by Parrish et al. (2020), so that they now have greater statistical significance. This indicates that the derived rate of decrease in baseline ozone concentrations in recent years, which is seen in all of the fitted curves, is no longer accelerating. The derived *b*, *c*, and *d* coefficient values in Table S1 generally agree within their confidence limits among the six data sets, which implies no statistically significant difference among the long-term changes derived from the six data sets, and these values are generally consistent with the *b* and *c* coefficient values in Table 2 of Parrish et al. (2020) that were derived from quadratic polynomial fits.

The magnitudes of the baseline ozone concentrations do differ significantly between data sets (cf. *a* parameter values in Table S1, which quantify the annual mean in the reference year 2000). These differences reflect the altitude dependence of baseline ozone concentrations, with the marine boundary layer data sets lower (33 and 40 ppb) than the FT data sets (51 to 58 ppb. The consistent long-term changes combined with significant differences in the absolute concentrations suggests normalizing all six data sets to allow more precise quantification of the common, overall long-term change. As in Parrish et al. (2020), we normalize each data set by subtracting its respective *a* parameter value, which gives the gray

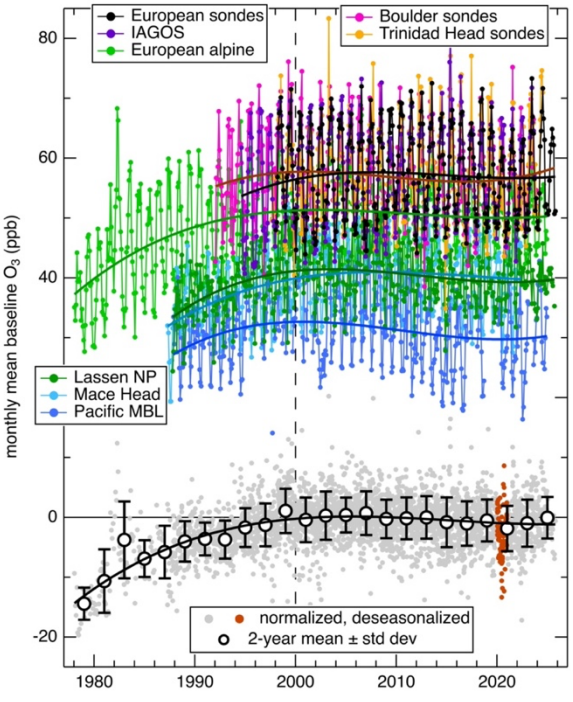

Figure 1: Time series of monthly mean (colored points) and normalized, deseasonalized monthly mean (gray and brown points) mixing ratios from all six long-term change data sets; the brown points are year 2020 data. The sonde and IAGOS data sets are 3-9 km altitude means. The symbols with error bars are 2-year means with standard deviations of the normalized, monthly means. The solid curves are the cubic polynomials from fits of Equation 1 to the monthly means (upper curves) and a cubic polynomial fit to the normalized monthly means (lower black curve). The vertical dashed line indicates the reference year 2000, the time origin for the functional fits.

https://doi.org/10.5194/egusphere-2026-1939
Preprint. Discussion started: 10 April 2026
© Author(s) 2026. CC BY 4.0 License.

and brown points in the lower graph of Fig. 1. The lower black solid curve is the regression fit of Equation 1 to all of those points. The upper part of Table 1 collects the derived parameter values, and compares the present results with those derived by Parrish et al. (2020). Averaging over the six baseline data sets and over two-year periods removes much of the spatial and temporal autocorrelation that is present in the normalized monthly means. A cubic polynomial fit to the two-year means provide wider, more realistic confidence limits, which are those included in Table 1. All parameter values agree within their respective confidence limits between the two studies.

Table 1. Parameter values (with 95% confidence limits) derived from fits to time series of deseasonalized, normalized, mean ozone concentrations from the eight baseline data sets.

parameter	this work	Parrish et al., 2020
fit of Equation 1 to normalized monthly means		
a (ppb)	-0.2 ± 0.8	-0.2 ± 1.0 *
b (ppb yr^{-1})	0.14 ± 0.10	0.21 ± 0.06 *
c (10^{-3} ppb yr^{-2})	-15 ± 4	-18 ± 6 *
d (10^{-4} ppb yr^{-3})	3.3 ± 2.7	(2 ± 6) ‡
year$_{max}$	2005.6 ± 5.1	2005.7 ± 2.5 *
RMSD (ppb)	3.7	4.0 *
years	1978-2025	1978-2018
number of data	3,220	2,563
linear fit to 2-year means		
Slope (all years) (ppb yr^{-1})	+0.19 ± 0.08	+0.27 ± 0.11
RMSD (ppb)	2.6	2.5
number of data	24	20
Slope (<2000) (ppb yr^{-1})	+0.59 ± 0.23§	+0.60 ± 0.23§
RMSD (ppb)	1.9	1.9
number of data	11	11
Slope (>2000) (ppb yr^{-1})	−0.053 ± 0.047	−0.093 ± 0.083
RMSD (ppb)	0.5	0.5
number of data	13	9

* Parrish et al. (2020) fit that included only the first 3 polynomial terms of Equation 1.
‡ Parrish et al. (2020) fit that included all 4 polynomial terms of Equation 1.

The year that baseline ozone concentrations at northern midlatitudes reached their maximum (year$_{max}$ derived from Equation 3 for the cubic fit) in the present work (2005.6 ± 5.1) agrees well with that derived from the quadratic fit to the shorter measurement record (2005.7 ± 2.5) by Parrish et al. (2020). Fig. S5 compares these fits; before 2016 the cubic and quadratic fits agree within < 0.8 ppb, but diverge significantly at later times. When the cubic term is included, the small differences in the b and c parameter values allow similar fits to the earlier data, while still allowing the cubic polynomial to closely fit the later data.

The piece-wise linear fits included in Fig. 2 provide an alternate, but consistent, quantification of the long-term baseline ozone changes. Over the 22 years before 2000 a marked increase occurred at an average rate of 5.9 ± 2.3 ppb per decade, followed over the next 26 years by a much slower decrease (trend = -0.53 ± 0.47 ppb per decade). Steinbrecht et al. (2025) review long-term changes of tropospheric ozone over Europe (see their Figs. 10 and 12), and find substantial increases from the 1960s to the early 1990s that are in at least qualitative accord with the rapid increase before 2000 found here. Van Malderen et al. (2025) derive trends for free troposphere ozone from measurements at 18 northern mid-latitude locations for the 2000-2022 period (their Table 2); the average of their derived trends is -0.08 ± 0.69 ppb per decade, indicating a smaller decrease, but agreeing with our result within specified confidence limits. Despite the non-linear behavior of the long-term changes, there has been a significant mean positive trend of +0.19 ± 0.08 ppb per year over the entire 48-year (1978-2025) record; however, as expected from the continuing decrease of baseline ozone during more recent years, this mean overall trend is smaller than the +0.27 ± 0.11 trend derived for the shorter 1978-1998 measurement record of Parrish et al. (2020).

https://doi.org/10.5194/egusphere-2026-1939
Preprint. Discussion started: 10 April 2026
© Author(s) 2026. CC BY 4.0 License.

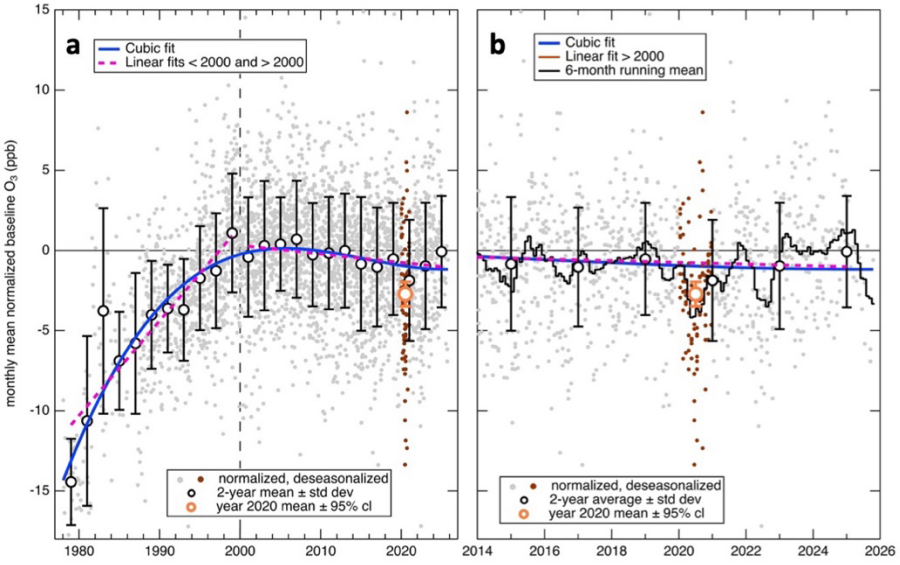

Figure 2: a) Lower part of Fig. 1 with expanded ordinate. Time series of normalized, deseasonalized monthly means (gray and brown points) from all eight data sets and the 2-year means with standard deviations are the same as in Fig. 1; the 2020 1-year mean with estimated confidence limits is included. Solid curve is cubic polynomial fit as in Fig. 1. The violet dashed lines are linear fits to the 2-year means before and after 2000. **b)** Most recent 12 years of **a)** on an expanded abscissa. Black stair-step line is 6-month running mean of normalized, deseasonalized monthly means.

3.2 Impact on baseline ozone during COVID-19 period

Efforts to control the COVID-19 pandemic through restrictions on societal activity led to reductions of anthropogenic ozone precursor emissions during 2020 throughout northern midlatitudes (e.g., Doumbia et al., 2021). These substantial reductions provide an opportunity to quantify the contribution that these emissions make to zonal baseline ozone concentrations. In Fig. 2 the year 2020 data are highlighted, both as normalized, deseasonalized monthly means, and as an annual mean. Three estimates are made - the April-August 2020 mean, the minimum of the 6-month running means (stairstep trace in Fig. 2b) and the 2020 annual mean are each compared to the baseline ozone expected from interpolation of the long-term change in mean baseline ozone discussed in Section 3.1. As summarized in the lower section of Table 2, the three estimates of the impact of the COVID-19 related emission reductions baseline ozone fall within the 1.7 to 4.1 ppb range, and agree within their confidence limits. Figure S5 shows that extrapolation of their quadratic fit to data through 2018 led Parrish et al. (2022) to underestimate that impact.

Table 2. Comparison of quantifications of COVID-19 related emission reduction impact on baseline ozone concentrations.

analysis assumption	ozone reduction	region	reference
April-August, 2020 vs. 2000–2020 climatological mean	7% (≈4 ppb)	Northern Hemisphere FT	Steinbrecht et al., 2021
2020 annual mean anomalies from 1994-2019 mean linear trend	3.6 ± 1.8 ppb 2.3 ± 1.9 ppb	Western Europe FT Western N. Amer FT	Chang et al., 2022
April-August, 2020 vs. extrapolated long-term O_3 decrease	1.2 ± 1.3 ppb	Northern midlatitude troposphere	Parrish et al., 2022
April-August, 2020 * Minimum 6-month running mean * Year 2020 annual mean *	4.1 ± 2.2 ppb 3.2 ± 2.0 ppb 1.7 ± 0.7ppb	Northern midlatitude troposphere	present work

* Reduction relative to the interpolated long-term O_3 decrease

https://doi.org/10.5194/egusphere-2026-1939
Preprint. Discussion started: 10 April 2026
© Author(s) 2026. CC BY 4.0 License.

3.3 Seasonal cycle of mean baseline ozone

The seasonal cycles for all eight baseline ozone data sets are quantified by the first two terms of the Fourier series, i.e., the final two terms of Equation 1, as illustrated in Fig. 3a. In the FT, Equation 1 is fit to the monthly means of each of the three sonde and IAGOS data sets averaged over the 3 to 4 km altitude interval to give results comparable to those from analysis of the European alpine data set, as those site elevations lie within that altitude interval. In the fits to these five data sets only the first term (the fundamental harmonic) is clearly statistically justified; there are indications of a small contribution from the 3rd (but not 2nd) harmonic, which is discussed in Section S5 of the Supplement. The fundamental and second harmonic are both statistically justified for the three lower elevation data sets. Parameters from the fits of these Fourier series terms are given in Table S2. Parrish et al. (2020) give a detailed discussion of the small numbers of Fourier series terms that are statistically justified for inclusion. The curves in Fig. 3a represent the mean seasonal cycles over the entire time span of the respective measurement records. The mean seasonal ozone changes for all eight baseline ozone data sets are shown in Fig. 3b; these curves illustrate the sums of the reference year 2000 intercepts (the *a* parameter values of Equation 1 given in Table S2) plus the seasonal cycles shown in Fig. 3a.

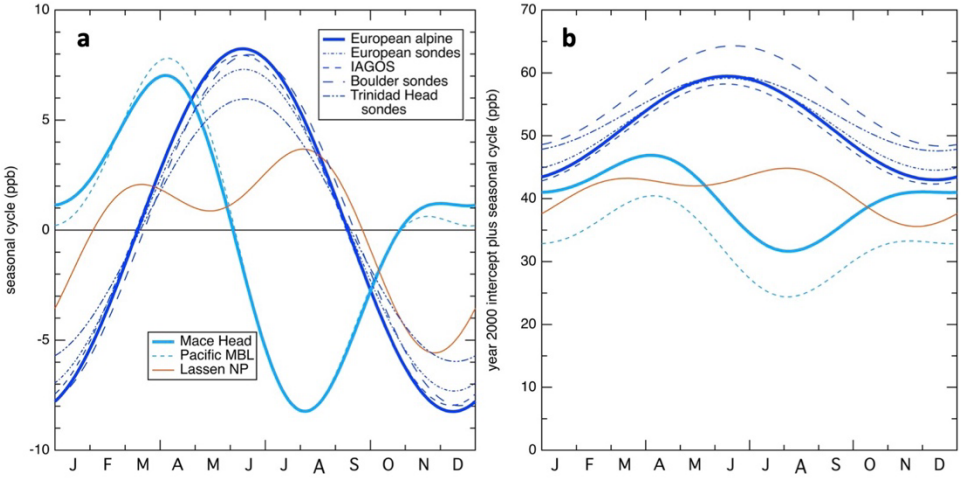

Figure 3: a) Seasonal cycles derived from eight baseline ozone data sets. Parameters of the Fourier series terms that define these cycles are given in Table S2. **b)** Sum of the reference year 2000 intercepts (*a* parameter values given in Table S2) and seasonal cycles shown **a)**.

3.4 Long-term shifts in seasonal cycle of baseline ozone

Fig. 4a shows that the ozone seasonal cycle at the European alpine sites has not remained constant. Its amplitude increased early in the measurement record, reached a maximum near 1990, and then decreased. The oscillating curve in Fig. 4a illustrates the fit of Equation 7 to the monthly means, with the derived parameter values annotated. That fit indicates that not only the amplitude, but also the phase of the seasonal cycle (i.e., the date of the seasonal maximum) shifted. An initial fit of Equation 6 to the monthly data indicated that the maximum amplitude of the seasonal cycle occurred in 1992 ± 7 years and the maximum of the phase shift occurred in 1986 ± 17 years. Since the year of the maximum shifts agrees within their confidence limits, the fit to Equation 7 is taken as providing the more precise and accurate analysis. Figure 4b illustrates five detrended seasonal cycles at 11-year intervals based on the fit to Equation 7. The shifts in the amplitude and phase of the seasonal cycle are readily apparent. The precision to which the shift of the seasonal cycle can be defined is relatively poor,

https://doi.org/10.5194/egusphere-2026-1939
Preprint. Discussion started: 10 April 2026
© Author(s) 2026. CC BY 4.0 License.

due to the large residual variability about the fitted curves. A fit to the mean seasonal cycle (i.e., Equation 1) has a root-mean-square deviation of 3.25 ppb, which is only reduced to 3.10 ppb by the fit to Equation 7. Similar shifts in the seasonal cycles in the data sets from other sites are presumed present, but we are unable to quantify them within significant statistical precision.

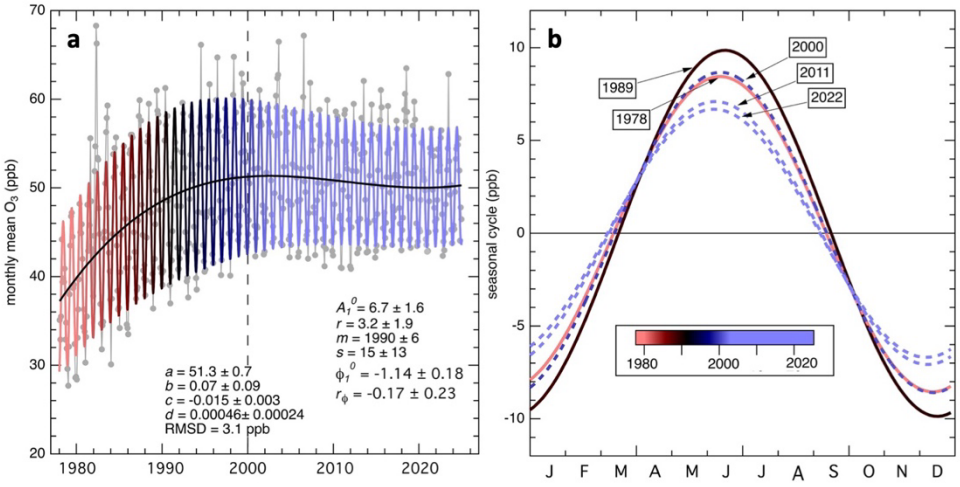

Figure 4: a) Time series of monthly mean mixing ratios (connected gray points) from the European alpine data set. The black and year color-coded curves are the cubic polynomial fit and the fit of Equation 7 to the monthly means, respectively. The parameter values (with the *m* value given as year) of the latter fit are annotated; units are discussed in the text. **b)** Detrended seasonal cycles derived from the two fitted curves in **a)**. Every eleventh year's seasonal cycle is shown, color-coded according to the annotation, as is the curve in **a)**. The three later year curves are plotted as dashed curves, so that the earlier solid curves can be more clearly discerned.

4 Discussion and conclusions

An underlying qualitative conceptual model of tropospheric ozone guides the analysis in this paper. This model has two primary features. First, in the background FT at mid-latitudes the ozone lifetime is long enough that the FT approximates a well-mixed reservoir. Mims et al. (2022) present a quantitative conceptual model that incorporates this picture, and Section S4 here applies that model to illustrate the validity of that approximation. This FT reservoir provides the dominant source of ozone to the MBL, but not necessarily the continental boundary layer. Consequently, analysis of a few long-term measurement records from FT and MBL baseline locations at northern mid-latitudes provides an accurate, zonally representative picture of the systematic long-term changes and seasonal cycles of baseline ozone. Section 3 discusses results supporting this picture. Second, mean ozone concentrations in the troposphere generally change only slowly, i.e., on decadal or longer time scales, because the mean source and sink magnitudes change slowly. Examples of such slowly changing sources and sinks are photochemical production from anthropogenic emissions, land use and climate change. (Such slow changes occasionally can be disrupted by relatively catastrophic events such as the COVID-19 pandemic or natural phenomena such as volcanic eruptions.) Simultaneously, seasonally repetitive changes in the magnitudes of sources and sinks impose a seasonal cycle about the long-term changes. Our analysis approach is optimized based on this conceptual model – a power series quantifies the slowly-varying long-term change with no assumption regarding the functional form of that change, and the Fourier series quantifies the repetitive seasonal cycle. Inclusion of only statistically significant terms in

https://doi.org/10.5194/egusphere-2026-1939
Preprint. Discussion started: 10 April 2026
© Author(s) 2026. CC BY 4.0 License.

both series ensures that the data are not over fit. (Due care must be taken to account for any catastrophic events that may have affected the measurements, as has been done for the COVID-19 period in this work.) Despite the well-mixed nature of the FT and the temporal inertia of ozone sources and sinks, monthly means of baseline ozone still exhibit more-or-less chaotic variability driven by meteorological cycles varying on time scales of weeks to decades or more. It is this residual ozone variability of 2 to 6 ppb (as quantified by the RMSD values of the monthly mean data from the fitted curves given in Table S2), that limits the accuracy and precision of our quantification of the long-term changes and seasonal cycles of baseline ozone.

4.1 Long-term changes in mean baseline ozone since the mid-20th Century

It is well established that rapid industrialization occurring during the last half of the 20th century at northern mid-latitudes markedly increased ozone during that period. As early as a meeting in June 1987 Paul Crutzen (1988) gave an overview of the then current knowledge of tropospheric ozone, describing increasing trends at northern mid-latitudes, and a guide for future analysis. Based on a comparison of his survey of historical measurement data from the 1930s through the 1950s with more recent data then available, he concluded that "… at more remote background stations (at northern mid-latitudes) substantial ozone increases have taken place", and noted that "it would be very interesting to compare certified old data with modern data taken at the same sites as where the 'ancient' data were taken." Subsequent analysis efforts have followed that guidance, e.g., Hough and Derwent (1990) and analysis conducted by the Task Force on Hemispheric Transport of Air Pollution (HTAP, 2010; Parrish et al., 2012; 2014). Notably, Logan et al. (2012) and Tarasick et al. (2019) have exhaustively examined uncertainties in measurement techniques employed over the decades, and thereby have effectively "certified" the old data. The analysis in this paper further extends Crutzen's original suggestion by comparing data sets collected at the same northern mid-latitude locations through the year 2025; these data sets now span nearly a half-century (48 years).

Over the past few years, a clear picture has come into focus. Parrish et al. (2020) showed that the well-mixed character of the FT leads to a nearly uniform long-term zonal change in baseline ozone; i.e., results obtained from measurements conducted at locations distributed vertically and longitudinally agree within their estimated confidence limits. Parrish et al. (2021b) showed that change amounted to an approximate doubling (increase of a factor of 2.1 ± 0.2) over the 1950–2000 period. That long-term increase ended during the first decade of the 21st century, followed by a slow decrease. In Section 3.1 the cubic polynomial analysis extends the quantification of the long-term change through 2025, and indicates the maximum was reached in 2005 ± 5 years. The piece-wise linear analysis quantifies a slow average decrease of 0.53 ± 0.47 ppb/decade over the 2000-2025 period; this result may indicate a slowing from the decrease of 0.93 ± 0.83 ppb/decade over the shorter 2000-2017 period derived by Parrish et al. (2020), although these two trends do agree within their confidence limits. Notably, the decrease after the year 2000 is much slower than the pre-maximum increase of 6 ± 2 ppb/decade over the 1978-2000 period. This asymmetry necessitates an analysis based on the cubic polynomial fit used here, rather than the quadratic fit used by Parrish et al. (2020). Note that some of the fits plotted in Figs. 1, 4a and S1-S4 appear to show that an increasing

https://doi.org/10.5194/egusphere-2026-1939
Preprint. Discussion started: 10 April 2026
© Author(s) 2026. CC BY 4.0 License.

trend may be developing during the last few years of measurements; however, this increase cannot be considered statistically significant, as it may be a misleading end effect of the cubic polynomial fit to those data sets.

4.2 Transitory decrease in baseline ozone due to precursor emission reductions during COVID-19 period

Disagreement remains among different quantifications of the influence of the COVID-19 emission reductions on northern mid-latitude baseline ozone. The upper section of Table 2 summarizes the results of three published studies. The differences in the results among these studies are primarily due to varying estimates of the 2020 baseline ozone concentrations that would have been measured in the absence of the COVID-19 impact. Table 2 shows that the present results are in agreement with those of Steinbrecht et al. (2021) and Chang et al. (2022), but indicate a larger decrease than the Parrish et al. (2022) estimate. That latter result underestimated the decrease due to extrapolation of the quadratic fit analysis of Parrish et al. (2020), which included data only through 2018; that extrapolation was approximately 2.3 ppb lower than the interpolation of the cubic fit to the presently available entire data record (see Fig. S5). Excluding the result of Parrish et al. (2022), the mean of six larger results in Table 2 is 3.1 ± 1.0 ppb, with the standard deviation indicated; we take this value as the best estimate of the magnitude and uncertainty of the baseline ozone decrease during the period of COVID-19 related emission reductions.

4.3 Mean seasonal cycle of baseline ozone and its long-term shift

Conceptually, we expect 1) the Fourier series fit to the seasonal cycle to yield only a small number of statistically significant terms, because the long effective ozone lifetime (i.e., the lifetime based on the difference in rates of formation and loss) in baseline air masses serves to damp out ozone variability on time scales shorter than a few months, and 2) similar seasonal cycles occur throughout northern mid-latitudes due to the circum-global transport time being shorter than the effective ozone lifetime. Differences in the seasonal cycle are expected between the FT, with the long effective ozone lifetime, and the MBL, where rapid ozone loss occurs in summer; the analysis results agree with these expectations. As illustrated in Fig. 3, indicated by the parameter values given in Table S2, and as fully discussed by Parrish et al. (2020), the fundamental harmonic makes the predominate contribution to the seasonal cycle in both the FT and the MBL, while the second harmonic makes a significant contribution in the MBL but not in the FT. Contributions from higher order harmonics are negligible (except for a small 3rd harmonic contribution at some FT sites – see Section S5 of the Supplement). Consequently, in Fig. 3a the fits to the seasonal cycle in the five FT data sets are pure sine functions, while the second harmonic contribution gives more complex behavior to the seasonal cycles in the MBL. The seasonal cycle at the Lassen NP site, located on the North American continent at a relatively low elevation (1.76 km), relatively near (~ 240 km inland) the Pacific coast, likely reflects transport of a mixture of both MBL and FT air impacted by dry deposition over the continent.

In both graphs of Fig. 3, the seasonal cycle curves of the five FT data sets (dark blue curves) are similar, and the derived amplitude (A_1) and phase (ϕ_1) parameter values for this single significant harmonic (the fundamental) generally agree within their confidence limits for all data sets (see Table S2). (The one exception is the amplitude derived for the Trinidad Head sondes, which is the data set that that was the latest to be initiated, and thus reflects measurements only after the seasonal

https://doi.org/10.5194/egusphere-2026-1939
Preprint. Discussion started: 10 April 2026
© Author(s) 2026. CC BY 4.0 License.

cycle amplitude had begun decreasing from its maximum - see discussion in Section 3.4). The curves for the two MBL sites (light blue curves) are also similar, although the annual mean ozone is larger by ~7 ppb at Mace Head than at the Pacific MBL sites. The analysis here is in accord with the conclusions of Parrish et al. (2020) that the mean seasonal cycle is similar at MBL sites and similar at common altitudes in the FT throughout northern mid-latitudes. The mean seasonal cycles at Mace Head and the European alpine sites (the heavier, light and dark blue curves in Fig. 3b) are those used by Mims et al. (2022) to characterize the seasonal dependence of mean baseline ozone in the MBL and FT, respectively.

Figure 4 illustrates the long-term shift of the seasonal cycle analyzed in Section 3.4. That shift is quantified as a change of the fundamental harmonic through a fit of Equation 7 to the longest measurement record, i.e., that from the European alpine sites. This fit indicates that the shift in the fundamental harmonic began before the 1978 start of measurements, maximized in 1990 ± 6 years, and by 2025 had nearly returned to that extrapolated to preindustrial times. The shift in the amplitude of the fundamental is relatively large – an increase of 3.2 ± 1.9 ppb from an unshifted amplitude of 6.7 ± 1.6 ppb, i.e., nearly a 50% increase. Concurrent with the amplitude shift, the phase of the fundamental also shifted – from an average seasonal maximum occurring on June 7 ± 10 days before industrialization to one occurring 10 ± 13 days later. This analysis is generally consistent with earlier discussions of shifts in the phase and amplitude of the mean seasonal cycle at northern mid-latitudes (see discussion and references in Bowman et al., 2022).

4.4 Challenges to our understanding of atmospheric chemistry

Chemistry Climate Models (CCMs) are designed to incorporate our complete understanding of atmospheric chemistry and transport processes so that all aspects of atmospheric composition can be simulated. Comparisons of observations to such simulation results, analyzed in the same manner as the observations are analyzed in Section 3, provide tests of our understanding of atmospheric chemistry, at least as that understanding is incorporated into those models. The analysis of the long-term changes and seasonal cycle in the 48-year record of northern mid-latitude baseline ozone presents several unmet challenges for CCM simulations.

Earth System Models (ESMs) incorporate CCMs to simulate the chemistry and transport within the atmosphere interacting with land and ocean in a fully coupled sense (Young et al., 2018). Here we analyze the tropospheric ozone concentration fields from historical (1850-2014) simulations conducted by six ESMs for the Coupled Model Intercomparison Project Phase 6 (CMIP6) (Eyring et al., 2016). Bowman et al. (2022) conducted the analysis of the ESM simulations, and we use results from that work as the basis for comparisons presented here. We take the results of these six models to be representative of ESM simulations in general, without discussion of the results from any specific model; the individual model simulations are identified by the acronyms used by Bowman et al. (2022), and that reference describes the models. One particularly useful aspect of the CMIP6 effort is that all models utilized a common time-dependent anthropogenic precursor emission data base and a common history of methane concentrations, which were specified in advance of the simulations. Bowman et al. (2022) integrated those emissions over northern mid-latitudes to provide the relevant time history of the emissions of the important

https://doi.org/10.5194/egusphere-2026-1939
Preprint. Discussion started: 10 April 2026
© Author(s) 2026. CC BY 4.0 License.

ozone precursors - the oxides of nitrogen (NOx = NO + NO_2) and non-methane volatile organic compounds (NMVOCs). We compare those time histories with measured and simulated long-term changes and seasonal cycles of baseline ozone.

Bowman et al. (2022) fit an equation similar to Equation 6 utilized in this work to time series of model simulations of monthly mean ozone concentrations. The one difference from Equation 6 above is that they included five, instead of four, power series terms (i.e., they used a 4th order polynomial) in order to provide adequate fits to the long-term ozone changes over the much longer 165-year CMIP6 simulation period. Here we compare the fits to the observations discussed in preceding sections with the fits to the model simulations to examine successes and short-comings of those simulations. Bowman et al. (2022) discussed the model simulations at six northern mid-latitude locations; here we focus on two of those locations: model cells at the location and elevation of the Jungfraujoch site (one of the three European alpine sites) and model cells at altitudes between 5 and 6 km above the Trinidad Head CA MBL site. Important points of agreement and informative points of disagreement are discussed in the following sections.

4.4.1 High bias of model simulations at northern mid-latitudes

Analysis of the long-term ozone changes from model simulations are compared with measurements at the European alpine sites in Fig. 5 and at the more remote, higher altitude FT location over Trinidad Head CA in Fig. S6. These figures show that models differ among themselves in their estimates of absolute baseline ozone concentrations, and are, on average, biased high with respect to the measurements. A positive bias of model simulations at northern mid-latitudes early in the 21st century has been noted previously, both for CCMs in general (e.g., Section 4.2 of Young et al., 2018) and the CMIP6 ESMs specifically, where an ensemble high bias of ~10% has been noted in the northern hemisphere (Griffiths et al., 2021). The fits to the measurements and model simulations in Fig. 5a allow bias estimation over the entire period of the measurements. Table 3 summarizes such estimates for the year 2000 at two locations (European alpine sites and in the FT above Trinidad Head); the differences between the model simulation and the measurements give an estimate of the model bias in that year. These results indicate a mean high model bias of ~5-6 ppb, i.e., ~8-12%, consistent with the analysis of Griffiths et al. (2021). However, the divergence between the fits to the measurements and model simulations in Fig. 5a indicates that the bias was significantly larger through the 20th century. This bias change can be approximately quantified by comparing the model simulations with historical measurements at the relatively high elevation European sites reviewed by Tarasick et al. (2019). Their Table 4 compiles measurement data collected at northern mid-latitude sites. Several of those sites are in Europe at elevations between 1.86 and 3.45 km, where measurements were conducted in two earlier decades of the 20th century - the 1950s and 1930s. These sites are thus comparable to the European alpine sites analyzed in this work, and provide a basis for extending that measurement record back to the 1930s. Table 3 gives the means of the Tarasick et al. (2019) data (Section S2 provides more details), and includes the quantified biases that result from comparison to model simulations. Those means are plotted in Fig. 5a. It is clear that the positive biases of the model simulations are much greater (~12 and 21 ppb, i.e., ~42 and 87%) in the 1930's and 1950s than in 2000. This comparison indicates that in recent years

https://doi.org/10.5194/egusphere-2026-1939
Preprint. Discussion started: 10 April 2026
© Author(s) 2026. CC BY 4.0 License.

model biases are relatively small, but those biases approached a factor of 2 in earlier decades, indicating a significant shortcoming in the model simulation of historical ozone concentrations at northern mid-latitudes.

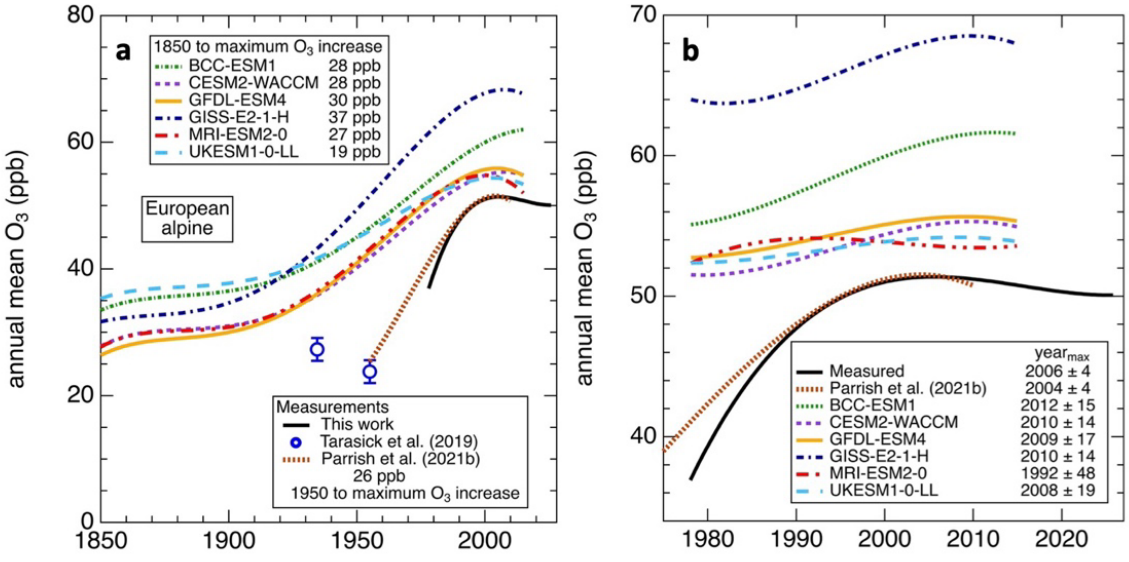

Figure 5: Long-term changes of baseline ozone quantified at the European alpine sites. The black curve illustrates the cubic polynomial fit to the normalized, deseasonalized monthly means from Fig. 1 offset by the reference year 2000 intercept (*a* parameter value = 51.3 ppb) derived in the analysis of European alpine data. Two measurement points from Tarasick et al. (2019) as discussed in Supplement Section S2 are included in **a)**. For comparison are fits to monthly mean ozone from six CMIP6 model simulations at the European alpine location (Bowman et al., 2022). In **a)** the model results are fit to a 5th order polynomial over the full 1850-2014 simulation period, and in **b)** to a cubic polynomial over 1978-2014. Included in both graphs is the cubic polynomial fit to annual mean ozone measured at 6 baseline-representative sites over the 1950 to 2010 period from Fig. 3 of Parrish et al. (2021b), also normalized to the European alpine *a* parameter value. The annotations in **a)** give the total increases of northern hemisphere baseline ozone over the full 1850-2015 simulation period of the models compared to the increase over the 1950 to 2000 period from the Parrish et al. (2021b) fit. The annotation in **b)** gives the years that the respective fits reached their maxima.

Table 3. Summary of model-measurement biases.

Location	year	measurements (ppb) mean ± 95% c.l.	Observations /reference	CMIP6 models (ppb) mean ± std. dev (range)	Model bias
European alpine	2000	51.3 ± 0.7	This work	57 ± 5 (54-67)	12%
Trinidad Head FT	2000	56.4 ± 1.3	This work	61 ± 6 (54-69)	8%
European alpine	1950s	23.8 ± 1.8	Tarasick et al. (2019)	45 ± 4 (41-51)	87%
European alpine	1930s	27.3 ± 1.8	Tarasick et al. (2019)	39 ± 3 (36-43)	42%

4.4.2 Comparison of simulated and observed long-term ozone changes

The CMIP6 ESM simulations of long-term ozone changes are in general agreement with measurements in two important regards: first, northern midlatitude baseline ozone concentrations approximately doubled over the simulation period, i.e., from pre-industrial levels to those in recent years, and second, those concentrations reached a maximum early in the 21st century. Figure 5 compares fits to measurements at the European alpine sites and ESM simulated long-term ozone changes at

https://doi.org/10.5194/egusphere-2026-1939
Preprint. Discussion started: 10 April 2026
© Author(s) 2026. CC BY 4.0 License.

model grid cells at the location and elevation of the Jungfraujoch station, one of the European alpine sites. Figure 5a shows 4th order polynomial fits to the monthly mean ozone simulated by the six ESMs over the entire simulation period. The annotation in Fig. 5a gives the ozone increase from 1850 to the maximum concentration from each model simulation. The mean ± standard deviation of the increase for the six models is 28 ± 6 ppb. Two derived fits to observations are included in both graphs in Fig. 5; one is over the 1978-2025 period derived in this work and illustrated in Figs. 1 and 2, and the other is over the 1950 to 2010 period from Parrish et al. (2021b). This latter observational-based fit gives an estimated factor increase of 2.1 ± 0.2 over the 1950-2000 period, which is taken as the best estimate for the increase in baseline ozone at northern mid-latitudes during the industrialization of the 20th century. This factor increase corresponds to an increase of 26 ± 3 ppb, which agrees well with the mean of the model simulations. Figure 5b shows the cubic polynomial fits to the simulated monthly mean ozone over 1978-2014, the period spanned by both the simulations and measurements; these fits give a better representation of the more recent long-term changes. The year of the occurrence of the maximum of each fit to the simulations and observations ($year_{max}$) are annotated in Fig. 5b. The weighted mean of the model simulations is 2010 ± 6 years, which agrees with the observational-based estimate of 2006 ± 4 years derived from the fit illustrated in Figs. 1 and 2. Bowman et al. (2022) conducted analyses of measured and simulated ozone concentrations at six baseline representative locations at northern mid-latitudes. Generally consistent results were found at all locations. For example, Fig. S6, in the same format as Fig. 5, illustrates the same analysis at a more remote location (5 to 6 km altitude above the North American Pacific Coast at Trinidad Head CA). The models simulated the same mean ozone increase of 28 ± 6 ppb and a similar weighted mean $year_{max}$ of 2013 ± 10 years. Overall, the model simulations exhibit considerable skill in reproducing the total ozone increase over the industrialization period and the $year_{max}$ of baseline ozone at northern mid-latitudes, despite the apparent differences in magnitude and shapes of the fitted curves among the models and between the models and the fit to the measurements.

The critical difference between the long-term baseline ozone changes quantified from the measurements and the simulations is the different time scales of the respective increases. The measurements indicate that baseline ozone concentrations remained near pre-industrial levels with little change until the 1950s, followed by a steep increase between 1950 and 2000. In contrast, model simulations find a more gradual increase extending over the entire 20th century. Figure 6 compares the fits to the measurements and to the ensemble mean of the simulations with the temporal evolution of tropospheric methane concentrations and anthropogenic NMVOC and NOx ozone precursor emissions at northern midlatitudes that were specified for the CMIP6 simulations. This comparison indicates that the observed baseline ozone concentrations approximately followed the long-term changes in the precursor emissions, particularly those of NOx. In contrast, the model simulations over the 1850-1950 period increased similarly to the methane concentrations. Beginning in ~1950, the model simulated relative increase ozone was slower than the corresponding increase in either the precursor emissions or methane. It is these differing shapes of the temporal increase of ozone that account for the changing model-measurement bias discussed in the preceding section.

https://doi.org/10.5194/egusphere-2026-1939
Preprint. Discussion started: 10 April 2026
© Author(s) 2026. CC BY 4.0 License.

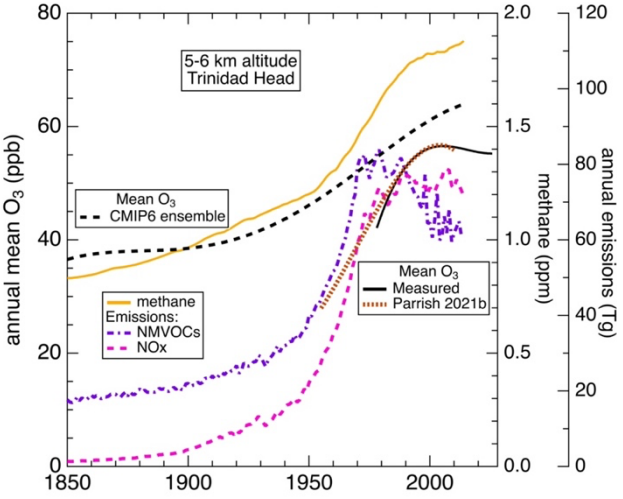

Figure 6: Model simulations and measurements of the long-term change of baseline ozone compared to methane concentrations and anthropogenic precursor emissions. The model simulation is the average of the fits to the six CMIP6 simulations for model grid cells located between 5 and 6 km altitude above Trinidad Head California as included in Fig. S6a. The measurements are normalized to the reference year 2000 intercept fit to mean baseline ozone measured over that altitude interval by sondes launched from Trinidad Head. The colored curves show the CMIP6 prescribed methane concentration (solid line) and total northern mid-latitude annual emissions of NMVOCs (dot-dash curve) and NOx (short-dashed curve) as discussed by Bowman et al. (2022).

4.4.3 Simulation of seasonal cycle and its shift

At the European alpine sites, the model simulations of the ozone seasonal cycle (Fig. 7a) scatter about the measured mean seasonal cycle. The harmonic analyses of the simulation results (illustrated in Fig. S7) agree with the measurement analysis that the fundamental harmonic dominates the seasonal cycle, with the second harmonic making only a secondary contribution. However, the model results vary considerably, both among themselves and relative to the observations. The timings of the simulated seasonal maxima vary over nearly three months (May 2 to July 21) compared to an observed maximum on June 12 ± 5 days, and the simulated peak-to-peak amplitudes vary between 12 and 34 ppb compared to an observed amplitude of 16.5 ± 1.5 ppb. In the FT at 5 to 6 km altitude above the North American Pacific Coast (Fig. 7b) the model simulations agree more closely with each other and with the observations. The timings of the simulated seasonal maxima agree within less than two months (May 3 to June 23) compared to June 10 ± 8 days from the observations, and the simulated peak-to-peak amplitudes vary between 11 and 19 ppb compared to 16 ± 3 ppb from the measurements. Figure S7 shows that some models simulate significant 2nd harmonics; at both locations there is little agreement regarding either the amplitude or phase of the 2nd harmonic, which accounts for the different shapes of the simulated seasonal cycles apparent in Fig. 7, and their deviation from pure sine functions.

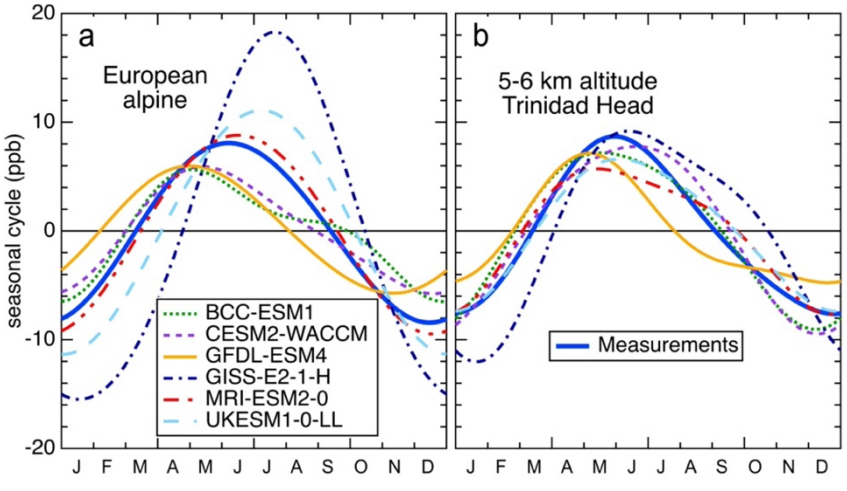

Figure 7: Baseline ozone seasonal cycles derived from measurements and model simulations at **a)** the European alpine sites and **b)** 5-6 km altitude above the North American Pacific Coast at Trinidad Head CA. The measurements are the European alpine data in **a)**, and the Trinidad Head CA sonde data in **b)**. The fits to the simulations begin in 1978, the initial year of the European alpine data.

https://doi.org/10.5194/egusphere-2026-1939
Preprint. Discussion started: 10 April 2026
© Author(s) 2026. CC BY 4.0 License.

Parrish et al. (2020) concluded that observed northern mid-latitude ozone seasonal cycles were similar in the FT throughout the entire zone at any specific altitude. As discussed in Section 4.3 and indicated by the parameter values given in Table S2, the present observational analysis is consistent with this conclusion, as exemplified by the two locations illustrated in Fig. 7. In contrast, for the most part the model simulations do not closely reproduce this high degree of zonal similarity, as again exemplified by the significant differences between the simulated seasonal cycles at the two locations in Fig. 7. Variability in the model simulations of similar or greater magnitudes is noted by Bowman et al. (2022) at all of the FT locations they examined. Overall, observations indicate that the mean FT ozone concentrations at northern mid-latitudes approximate a well-mixed reservoir with little systematic spatial variability beyond the average seasonal cycle and altitude gradient, but model simulations generally do not capture this zonal uniformity. We hypothesize that the simulation of the convective boundary layer over Europe is too "leaky" in at least some models, i.e., Fig. 7a shows that the simulation of the continental boundary layer allows too much boundary layer influence to reach the European alpine sites, which sample in the overlying free troposphere. The boundary layer influence at the more remote and higher (5 to 6 km altitude) FT location above the North American Pacific Coast (Fig. 7b) is smaller and consistent with the analysis of Parrish et al. (2016); they analyzed the same sonde data set, and found a strong isolation of the MBL seasonal cycle below ~1 km altitude, while the models simulate the influence of the MBL seasonal cycle extending into the FT to altitudes above 3 km. Parrish et al. (2016) concluded that the treatment of MBL dynamics in three CMIP5 GCMs was not adequate to reproduce the observed isolation of the Trinidad Head MBL seasonal cycle, and here we reach a similar conclusion over the continents.

Bowman et al. (2022) document that the shift of the ozone seasonal cycle in the FT is qualitatively reproduced by the overall average of the six CMIP6 model simulations considered here (see their Fig. 8), although they found substantial variation among the individual model simulations. Figure 8 here compares the average simulation of the seasonal cycle shift at the European alpine sites with the result derived from measurements in Section 4.3; the figure includes the temporal variation of the integrated northern mid-latitude NMVOC and NOx ozone precursor emissions (Bowman et al., 2022). Table 4 compares the parameter values derived in the fits to the simulations and measurements, and includes the summary of the seasonal shift derived from observations by Bowman et al. (2022). The years that the shifts of the amplitude and phase reached their maxima (*m* parameter values) agree within their

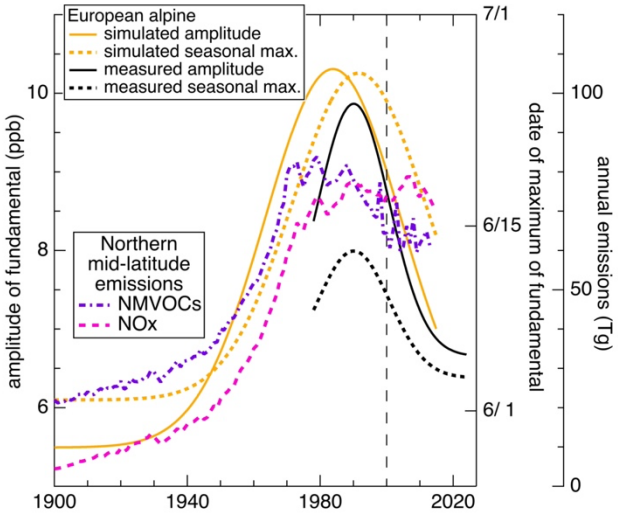

Figure 8: Observed shifts of the phase and amplitude of the fundamental harmonic of the ozone seasonal cycle (black curves) at the European alpine sites quantified by the Gaussian function parameter values derived in the fit of Equation 7 as illustrated in Fig. 4. The gold colored curves are similar results for the average of CMIP6 model simulations. The two lower dashed curves give the total northern mid-latitude annual emissions of NMVOCs and NOx as discussed by Bowman et al. (2022).

https://doi.org/10.5194/egusphere-2026-1939
Preprint. Discussion started: 10 April 2026
© Author(s) 2026. CC BY 4.0 License.

confidence limits between the average of the simulations and the observational analyses derived in Fig. 8. However, the magnitude of the shifts of the amplitude and phase (*r* parameter values) are overestimated by factors of 1.5 and 2.6, respectively, by the simulation average. The simulations also overestimate the time constant for growth and decay of the shifts (*s* parameter values) by a factor of 1.8. Individual model simulations have larger discrepancies; the derived *s* and *m* parameter values span factors of 2.2 and 5.8, respectively, at the European alpine Jungfraujoch site (Bowman et al., 2022). Overall, accurate and consistent model simulation of the baseline ozone seasonal cycle and its long-term shift remains an unmet challenge for CCMs.

Table 4. Gaussian parameters that define shifts in the amplitude and phase of the ozone seasonal cycle fundamental harmonic at the European alpine sites. The first row gives the average and standard deviation of the parameter values for fits to the six model simulations, while the second row gives the range of those values

	Preindustrial		**Gaussian maximum, *m* parameter**		**Gaussian amplitude, *r* parameter**		**Gaussian width, *s* parameter**	
	Amplitude (ppb)	Phase (rad)	Amplitude (Year)	Phase (Year)	Amplitude (ppb)	Phase (days)	Amplitude (year)	Phase (year)
Simulations [a]	5.5 ± 3.3	-1.11 ± 0.53	1984 ± 4	1992 ± 7	4.8 ± 0.9	25 ± 16	29 ± 7	28 ± 9
range	3 to 12	-0.4 to -1.8	1978 to 1988	1988 to 2002	2.3 to 7.4	8 to 46	21 to 38	19 to 41
Measurements [b]	6.7 ± 1.6	-1.14 ± 0.18	1990 ± 6	1990 ± 6	3.2 ± 1.9	10 ± 13	15 ± 13	15 ± 13
N. mid-latitude [c]	---	---	1990 ± 3	1985 ± 8	2.9 ± 1.4	14 ± 8	15 ± 9	17 ± 17

[a] Mean and standard deviation over all six model simulations discussed by Bowman et al. (2022).
[b] Results from fit of Equation 7 to the European alpine data set, so *m* and *s* parameters are the same for the amplitude and phase.
[c] Observational analysis results from Bowman et al. (2022) for Hohenpeissenberg and European alpine data records taken from their Table 3. The preindustrial amplitude and phase at the two sites differ, so values for these parameters are not included.

4.4.4 Relationship between long-term change and seasonal cycle shift.

At northern mid-latitudes the baseline ozone concentrations and the seasonal cycle of those concentrations have both changed over past decades, and both have been attributed to zonal changes in ozone precursor emissions. However, it is apparent that these changes are not well-correlated. Analysis of observations shows that the long-term ozone increase began ~1950 and reached a maximum in the middle of the decade of the 2000s (Figs. 5 and S6 and Table 1). There are no available data sets adequate for accurately characterizing changes in the seasonal cycle before the 1970s; however, the Gaussian fit to the temporal evolution of the seasonal cycle shift (Fig. 8 and Table 4) suggests that the seasonal shift was small in 1950, i.e., about 0.5 ppb added to the pre-industrial fundamental amplitude of 6.3 ppb. Comparison of Figs. 6 and 8 indicates that the long-term increase and the shift in the seasonal cycle of baseline ozone both correlated with the precursor emission increase through the last half of the 20th century, reaching maxima near the turn of the century. However, in the last two to three decades the shift in the seasonal cycle decreased strongly to the point that it now approximates that of preindustrial conditions, even though precursor emissions have remained near their maxima. In contrast, baseline ozone concentrations have decreased only slowly, and are presently elevated well above preindustrial levels. No specific cause has been established for the disappearance of the shift in the seasonal cycle of baseline ozone at northern mid-latitudes – it can be

https://doi.org/10.5194/egusphere-2026-1939
Preprint. Discussion started: 10 April 2026
© Author(s) 2026. CC BY 4.0 License.

speculated that the equatorward shift of anthropogenic precursor emissions (Zhang et al., 2016) and/or the changing climate (Schnell et al., 2016) may play a role. Importantly, the model simulations do qualitatively capture the lack of correlation between the continuing elevation of baseline ozone and the disappearing shift of the seasonal cycle.

4.5 Temporal evolution of zonal mean ozone production efficiency (OPE)

We examine possible cause of the long-term change of baseline ozone at northern mid-latitudes by applying a previously published simple compartmental model (Mims et al., 2022) that simplistically represents the ozone budget in the northern mid-latitudes. That zone is divided into 9 longitudinal regions - 4 marine and 5 continental - and each region contains a boundary layer and an overlying FT compartment, both assumed to be individually well mixed. The FT circulates west to east with an average circum-global transport time of 23 days, while sources and sinks are confined to the underlying boundary layer compartments that exchange with the overlying free troposphere as it passes over. This model was able to simultaneously match the average seasonal behavior of FT and MBL ozone measured at the European alpine sites and Mace Head, respectively, while predicting reasonable continental boundary layer behavior (Mims et al., 2022).

Relevant to this paper, changes in the regional distribution of ozone precursor emissions, which the model confines to the 5 continental BL compartments, cause changes in regional ozone production, which the model also confines to the continental BL. Any change in any continental BL ozone concentration affects ozone concentrations in all FT and BL compartments due to BL-FT exchange and FT circulation. Over the past decades there has been a major shift in the regional distribution of anthropogenic ozone precursor emissions and therefore in ozone production. Figure 9 shows that the eastern Asia compartment has replaced North America and Europe as the region of greatest NOx emission, and emissions in central Asia are now comparable to those in North America and Europe. The model was run for the five decadal years to simulate production from these emission distributions and to examine the effects of this emission shift. The photochemical ozone production was proportioned to the NOx emissions within each continental boundary layer compartment and the total production and its seasonal cycle adjusted to match the measured European free troposphere behavior - both its annual average and seasonal cycle - as given by the European alpine monthly mean data discussed in earlier sections. Figure S8 shows the temporal evolution of the

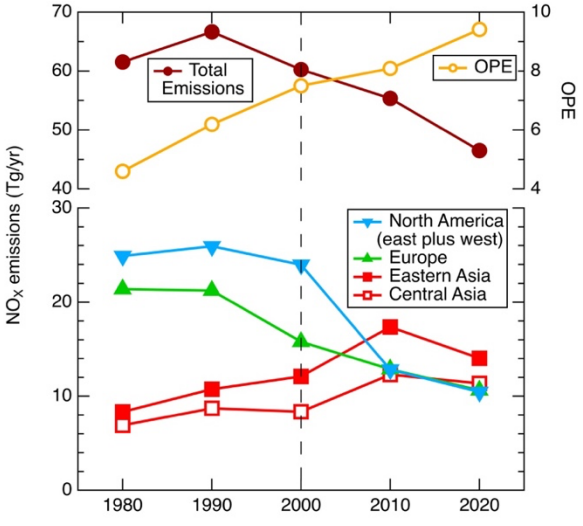

Figure 9. (lower graph) Temporal history of total (anthropogenic plus natural) NOx emissions into the 5 continental boundary layer model compartments at northern mid-latitudes derived from the EDGAR emissions database. The data points are 5-year averages around the fiducial years. North American emissions are divided equally between the eastern and western model compartments. **(upper graph)** Comparison of total northern mid-latitude NOx emissions and the model calculated mean ozone production efficiency (OPE).

https://doi.org/10.5194/egusphere-2026-1939
Preprint. Discussion started: 10 April 2026
© Author(s) 2026. CC BY 4.0 License.

model simulated baseline ozone concentrations for the 9 FT and 4 MBL compartments. The temporal evolution of the model simulated ozone concentrations in the 5 continental BL compartments (not shown) is more complex due to the interplay of ozone production within the compartment and transport (via the FT) from other BL compartments.

The zonal mean ozone production efficiency (OPE) simulated by the simple compartmental model are included in Fig. 9. The OPE values are derived from the sum of the ozone produced in all model compartments divided by the total zonal NOx emissions. Over the decades the OPE values are in the range of 4 to 10 molecules ozone produced per NOx molecule emitted, consistent with experimental studies of OPE in rural continental environments, e.g. OPE = 4 to 8 in different seasons at an eastern Massachusetts site (Hirsch et al., 1996) and OPE averages of 5.9 ± 1.2 in summer downwind of the Houston Texas region (Neuman et al., 2009). These model results indicate that the zonal mean OPE has approximately doubled in the 4-decade 1980 to 2020 period. The decrease in the total NOx emissions and the marked dilution of those emissions across all continental boundary layer compartments are qualitatively consistent with models (e.g., Liu et al., 1987), which simulate higher OPE at more dilute NOx concentrations. These regional mean OPE values may serve as useful benchmarks for evaluating CTM simulations of global ozone production.

4.6 Hypothesis: Uncertainty in NOx concentration field limits current model simulations

The comparisons in preceding sections show that model simulations of baseline ozone at northern mid-latitudes have significant shortcomings. The multitude and complexity of the chemical and physical processes that affect ozone contribute both to the difficulty of developing models that accurately simulate tropospheric ozone and to the difficulty of identifying and evaluating the causes of model shortcomings. The large spatial and temporal variability of the concentrations of critical atmospheric trace species contributes to the difficulty of assessing the performance of CCM simulations through comparison with atmospheric measurements. This difficulty is exacerbated for many critical species by their very low concentrations that challenge measurement capabilities.

One difficulty that is particularly critical for assessing simulations of tropospheric ozone is comparison of the simulated NOx concentration field to observations. The predominant in situ source of ozone in the background troposphere is the photochemical oxidation of methane and CO in the presence of NOx (see brief, simplified discussion of the relevant atmospheric photochemistry in Section S6 of the Supplement). However, at low enough NOx concentrations, this photochemistry results in net destruction of ozone instead of production. The break-even point for ozone is determined when hydroperoxy (HO_2) radicals react at equal rates with NO and ozone. This equality is reached when the diurnal mean concentration of NO is ~8 ppt, which corresponds to approximately 20 to 40 ppt NOx, depending upon ambient conditions. NOx concentrations in the background troposphere are not well-characterized, partly because the instruments generally deployed in field studies in the remote troposphere have been inadequate to accurately and precisely measure such low concentrations. Based on the temporally varying, high bias of simulated versus measured baseline ozone concentrations discussed in Section 4.4.1, and in the absence of persuasive comparisons of measured and simulated NOx concentration fields, we hypothesize that model simulations are consistently too NOx-rich in the background troposphere over at least the

https://doi.org/10.5194/egusphere-2026-1939
Preprint. Discussion started: 10 April 2026
© Author(s) 2026. CC BY 4.0 License.

past two centuries. Model simulations indicate that increasing methane concentrations increase ozone concentrations in the background troposphere (Fiore et al., 2008; Wild and Palmer, 2008); however, this may be incorrect. The average net ozone production in the troposphere is a small difference between much larger gross production and loss terms, so an overestimate in the simulated NOx concentrations in the background troposphere may cause only small errors in the simulated gross production and loss terms, but still lead to significant overestimates of the net ozone production. These two considerations imply that a methane increase could increase gross ozone destruction more than gross ozone production, with a resulting decrease in net ozone production and a decrease, rather than an increase, in baseline ozone concentrations. Given the significant differences between the measurements and model simulations of the long-term changes of baseline ozone discussed in Section 4.4.2, we believe that the role of methane in photochemical production of baseline ozone must be re-assessed with careful attention to the uncertainties of simulated NOx concentration fields.

We can identify two aspects of the simulation of NOx concentrations in CCMs that are particularly uncertain. First, the large majority of NOx emissions are localized in the continental boundary layer and the significant NOx emissions from shipping are localized in the MBL. Our evaluation of seasonal cycle simulations in Section 4.4.3 indicates that current model simulations of transport from the boundary layer to the FT allow too much boundary layer influence on ozone in the lower FT. That transport would also move too much NOx, as well as its organic nitrate reservoir species, to the lower FT, thereby contributing to overestimates in simulated FT NOx concentrations. Second, within the MBL and FT the primary in situ NOx emissions are highly localized in ship plumes in the MBL, and in aircraft exhaust plumes and paths of lightning strokes in the FT. At high concentrations NOx lifetimes are short with respect to plume dilution, but model simulations generally dilute these emissions through grid cells that are very large compared to plume dimensions. The treatment of ship emission plumes in the MBL has been evaluated in detail. Kasibhatla et al. (2000) suggested that that there is a gap in our understanding of the chemical evolution of the plumes as they mix into the background MBL. To address that gap, Chen et al. (2005) conducted an observation-based characterization of ship plume evolution and found that the photochemical perturbation of the MBL is largely limited to the first few hours following emission, while the plume was still well confined (full width at half maximum ~3 km). Thus, an effective model resolution on the order of 0.1 km is required to accurately simulate the photochemical evolution of ship emissions; global models generally lack such detailed resolution. Duncan et al. (2008) further evaluate this issue. To our knowledge, similar issues remain inadequately investigated for the photochemistry of dispersing aircraft and lightning stroke plumes in the FT. These considerations lead us to hypothesize that significant errors arise in model simulations of ozone due to inadequate simulation of the NOx concentration field, specifically an overestimate of NOx in the background troposphere.

5 Implications for utilizing model simulations

Despite their frequent use in such manner in published studies, the current generation of CCMs and ESMs, when used alone, are not tools that can simulate the atmosphere realistically enough to provide reliably accurate answers to questions

https://doi.org/10.5194/egusphere-2026-1939
Preprint. Discussion started: 10 April 2026
© Author(s) 2026. CC BY 4.0 License.

often posed for them. For example, if models cannot yet accurately simulate past changes of tropospheric ozone, it is unrealistic to expect those same models to accurately predict future ozone changes. Instead, the aphorism generally attributed to George Box provides sage guidance: "**All models are wrong, but some are useful**". CCMs and ECMs are useful – they are indispensable tools for organizing our atmospheric knowledge, and for providing state-of-the-art simulations of atmospheric composition. They can be used in a wide variety of heuristic efforts to expand our understanding of the atmosphere. For example, they could be used to investigate how historical increases in methane concentrations would have affected baseline ozone under differing simulations of the NOx concentration field. However, these models themselves are neither reality itself nor perfect simulations thereof. In this regard, a hierarchy of models is required to fully understand tropospheric composition (e.g., see Derwent et al., 2023) just as a model hierarchy has been identified as needed in climate modelling (e.g., see Held, 2005). The complexity of useful tropospheric composition models extends from the simplest conceptual models, such as that of Mims et al. (2022) utilized in this paper in Section 4, to the most sophisticated ESMs. Only when such a hierarchy can converge on consistent simulations of the atmosphere can we develop confidence that we are approaching a realistic understanding of the atmosphere. Perhaps a trivial analogy from meteorological forecasting, an endeavor that is in many respects simpler than simulating atmospheric composition, can demonstrate the utility of a model hierarchy. We are blessed with atmospheric models that predict coming weather days to weeks in advance with high reliability; nevertheless, even when fair weather is forecast, the more prudent among us consult our own mental conceptual model of weather when we leave home - if we observe that dark clouds are building, we return to grab an umbrella.

Acknowledgments

I.C. Faloona's effort was supported by the USDA National Institute of Food and Agriculture, (Hatch project CA-D-LAW-2481-H, "Understanding Background Atmospheric Composition, Regional Emissions, and Transport Patterns Across CA").

The authors are extremely grateful to the many researchers who sustained high quality measurement programs over the past 5 decades; without this enormous effort, which accumulated the 15 total measurement data sets considered here, it would not be possible to quantify northern mid-latitude baseline ozone in the troposphere. Brief descriptions and references to all data sets are given in Section 2.1.

Makoto Deushi and Naga Oshima were supported by the Environment Research and Technology Development Fund (JPMEERF20232001) of the Environmental Restoration and Conservation Agency provided by Ministry of the Environment of Japan, the Arctic Challenge for Sustainability 3 (ArCS-3) (JPMXD1720251001), and a grant for the Global Environmental Research Coordination System from Ministry of the Environment of Japan (MLIT2253).

Tongwen Wu and Jie Zhang provided model output from Beijing Climate Center (2019) WCRP CMIP6: Beijing Climate Center (BCC) BCC-ESM1 model output for the "historical" experiment. Centre for Environmental Data Analysis. https://catalogue.ceda.ac.uk/uuid/28deebaec6f447569569f27e1225ccdf.

https://doi.org/10.5194/egusphere-2026-1939
Preprint. Discussion started: 10 April 2026
© Author(s) 2026. CC BY 4.0 License.

Steven Turnock and Fiona M. O'Connor provided model output from Met Office Hadley Centre (2019): WCRP CMIP6: Met Office Hadley Centre (MOHC) UKESM1-0-LL model output for the "historical" experiment. Centre for Environmental Data Analysis. https://catalogue.ceda.ac.uk/uuid/59c10ac7bea2424f8eb64f0e310a2d4f.

The authors are grateful to the Earth System Grid Federation (https://esgf.llnl.gov) for archiving the CMIP6 model simulation results, and making them available to the scientific community.

Competing Interests

The contact authors have declared that none of the authors has any competing interests.

Author contributions

D.D.P. was responsible for the overall study design, observational data analysis and wrote the paper with input from C.A.M. and R.G.D. C.A.M. performed model analysis. All authors edited and revised the manuscript.

Data availability statement

All data analyzed for this paper are publicly available, as detailed in Section 2.1. The model simulation results also are publicly available, as detailed by Boman et al. (2022).

References

Bowman, H., Turnock, S., Bauer, S.E., Tsigaridis, K., Deuchi, M., Oshima, N., O'Connor, F.M., Horowitz, L., Wu, T., Zhang, J., Kubistin, D., Parrish, D.D.: Changes in anthropogenic precursor emissions drive shifts in the ozone seasonal cycle throughout the northern midlatitude troposphere, Atmos. Chem. Phys., 22, 3507–3524, https://doi.org/10.5194/acp-22-3507-2022, 2022.

Chang, K.-L., Cooper, O. R., Gaudel, A., Allaart, M., Ancellet, G., Clark, H., Godin-Beekmann, S., Leblanc, T., Van Malderen, R., Nédélec, P., Petropavlovskikh, I., Steinbrecht, W., Stübi, R., Tarasick D. W., and Torres, C.: Impact of the COVID-19 economic downturn on tropospheric ozone trends: An uncertainty weighted data synthesis for quantifying regional anomalies above western North America and Europe. AGU Advances, 3, e2021AV000542. https://doi.org/10.1029/2021AV000542, 2022.

Chen, G., Blake, D. R., Heikes, B., Huey, G., Lueb, R., Ryerson, T. B., Thornton, D., and Williams, E.: An investigation of the chemistry of ship emission plumes during ITCT 2002, J. Geophys. Res., 110, D10S90, https://doi.org/10.1029/2004JD005236, 2005.

https://doi.org/10.5194/egusphere-2026-1939
Preprint. Discussion started: 10 April 2026
© Author(s) 2026. CC BY 4.0 License.

Crutzen, P. J.: Tropospheric ozone: An overview, in: Isaksen, I. S. A. (Ed.), Tropospheric Ozone, NATO ASI Series, Vol. 227, Springer, Dordrecht, https://doi.org/10.1007/978-94-009-2913-5_1, 1988.

Derwent, R. G., Parrish, D. D., and Faloona, I. C.: Opinion: Establishing a science-into-policy process for tropospheric ozone assessment, Atmos. Chem. Phys., 23, 13613–13623, https://doi.org/10.5194/acp-23-13613-2023, 2023.

Derwent, R.G., Parrish, D.D., Simmonds, P.G., Manning, A.J., Spain, T.G., Simmonds, P.G., and S. O'Doherty: Ozone at Mace Head, Ireland from 1987 to 2021: Declining baselines, phase-out of European regional pollution, COVID-19 impacts, Atmos. Environ., 320, 120322, https://doi.org/10.1016/j.atmosenv.2023.120322, 2024.

Doumbia, T., Granier, C., Elguindi, N., Bouarar, I., Darras, S., Brasseur, G., Gaubert, B., Liu, Y., Shi, X., Stavrakou, T., Tilmes, S., Lacey, F., Deroubaix, A., and Wang, T.: Changes in global air pollutant emissions during the COVID-19 pandemic: a dataset for atmospheric modeling, Earth Syst. Sci. Data, 13, 4191–4206, https://doi.org/10.5194/essd-13-4191-2021, 2021.

Duncan, B. N., West, J. J., Yoshida, Y., Fiore, A. M., and Ziemke, J. R.: The influence of European pollution on ozone in the Near East and northern Africa, Atmos. Chem. Phys., 8, 2267–2283, https://doi.org/10.5194/acp-8-2267-2008, 2008.

Eyring, V., Bony, S., Meehl, G. A., Senior, C. A., Stevens, B., Stouffer, R. J., and Taylor, K. E.: Overview of the Coupled Model Intercomparison Project Phase 6 (CMIP6) experimental design and organization, Geosci. Model Dev., 9, 1937–1958, https://doi.org/10.5194/gmd-9-1937-2016, 2016.

Fiore, A. M., West, J. J., Horowitz, L. W. , Naik, V. and Schwarzkopf, M. D.: Characterizing the tropospheric ozone response to methane emission controls and the benefits to climate and air quality, J. Geophys. Res., 113, D08307, doi:10.1029/2007JD009162, 2008.

Griffiths, P. T., Murray, L. T., Zeng, G., Shin, Y. M., Abraham, N. L., Archibald, A. T., Deushi, M., Emmons, L. K., Galbally, I. E., Hassler, B., Horowitz, L. W., Keeble, J., Liu, J., Moeini, O., Naik, V., O'Connor, F. M., Oshima, N., Tarasick, D., Tilmes, S., Turnock, S. T.,Wild, O., Young, P. J., and Zanis, P.: Tropospheric ozone in CMIP6 simulations, Atmos. Chem. Phys., 21, 4187–4218, https://doi.org/10.5194/acp-21-4187-2021, 2021.

Held, I. M.: The gap between simulation and understanding in climate modeling, B. Am. Meteorol. Soc., 86, 1609–1614, https://doi.org/10.1175/Bams-86-11-1609, 2005.

Hirsch, A. I., Munger, J. W., Jacob, D. J., Horowitz, L. W., and Goldstein, A. H.: Seasonal Variation of the Ozone Production Efficiency Per Unit NOx at Harvard Forest, Massachusetts, J. Geophys. Res., 101 (D7): 12659-12,666, doi:10.1029/96jd00557, 1996.

Hough, A. M., and Derwent, R. G.: Changes in the global concentration of tropospheric ozone due to human activities, Nature, 344, 645–650, 1990.

HTAP: Hemispheric Transport of Air Pollution 2010, Part A: Ozone and Particulate Matter, Air Pollution Studies No. 17, edited by: Dentener F, Keating T, and Akimoto H, United Nations, New York and Geneva, 2010.

https://doi.org/10.5194/egusphere-2026-1939
Preprint. Discussion started: 10 April 2026
© Author(s) 2026. CC BY 4.0 License.

Kasibhatla, P., Levy II, H., Moxim, W.J., Pandis, S.N., Corbett, J.J., Peterson, M.C., Honrath, R.E., Frost, G.J., Knapp, K., Parrish, D.D., and Ryerson T.B.: Do emissions from ships have a significant impact on concentrations of nitrogen oxides in the marine boundary layer?, Geophysical Research Letters, 27 (15), 2229-2232, 2000.

Liu, S. C., Trainer, M., Fehsenfeld, F. C., Parrish, D. D., Williams, E. J. Fahey, D. W., Hübler, G. and Murphy, P. C.: Ozone production in the rural troposphere and the implications for regional and global ozone distributions, J. Geophys. Res., 92, 4191-4207, doi:10.1029/JD092iD04p04191, 1987.

Logan, J. A., Staehelin, J., Megretskaia, I. A., Cammas, J.-P., Thouret, V., Claude, H., De Backer, H., Steinbacher, M., Scheel, H. E., Stübi, R., Fröhlich, M., and Derwent, R.: Changes in ozone over Europe: analysis of ozone measurements from sondes, regular aircraft (MOZAIC) and alpine surface sites, J. Geophys. Res., 117, D09301, https://doi.org/10.1029/2011JD016952, 2012.

Mims, C.A., Parrish, D.D., Derwent, R.G., Astaneh, M., and I.C. Faloona: A conceptual model of northern midlatitude tropospheric ozone, Environ. Sci.: Atmos., 2, 1303-1313, DOI: 10.1039/d2ea00009a, 2022.

Neuman, J.A., Nowak, J.B., Zheng, W., Flocke, F.M., Ryerson, T.B., Trainer, M., Holloway, J.S., Parrish, D.D., Frost, G.J., Peischl, J., Atlas, E.L., Bahreini, R., Wollny, A., and Fehsenfeld, F.C.: Relationship between photochemical ozone production and NOx oxidation in Houston, Texas, J. Geophys. Res., 114, D00F08, doi:10.1029/2008JD011688, 2009.

Parrish, D.D., Millet, D. B., and Goldstein, A.H.: Increasing ozone in marine boundary layer air inflow at the west coasts of North America and Europe, Atmospheric Chemistry and Physics, 9, 1303–1323, 2009.

Parrish, D.D., Law, K. S., Staehelin, J., Derwent, R., Cooper, O. R., Tanimoto, H., Volz-Thomas, A., Gilge, S., Scheel, H.-E., Steinbacher, M., and Chan, E.: Long-term changes in lower tropospheric baseline ozone concentrations at northern mid-latitudes, Atmos. Chem. Phys., 12, 11485–11504, 85 https://doi.org/10.5194/acp-12-11485-2012, 2012.

Parrish, D.D, Lamarque, J.-F., Naik, V., Horowitz, L., Shindell, D.T., Staehelin, J., Derwent, R., Cooper, O.R., Tanimoto, H., Volz-Thomas, A., Gilge, S., Scheel, H.-E., Steinbacher, M. and Fröhlich, M.: Long-term changes in lower tropospheric baseline ozone concentrations: Comparing chemistry-climate models and observations at northern midlatitudes. J. Geophys. Res.: Atmos. 119:5719–5736, 2014.

Parrish, D. D., Galbally, I. E., Lamarque, J. -F., Naik, V., Horowitz, L., Shindell, D. T., Oltmans, S. J., Derwent, R., Tanimoto, H., Labuschagne, C., and Cupeiro, M.: Seasonal cycle of O_3 in the marine boundary layer: Observation and model simulation comparisons, J. Geophys. Res.-Atmos., 121, 538-557, https://doi.org/10.1002/2015JD024101, 2016.

Parrish, D. D., Derwent, R. G., O'Doherty, S., and Simmonds, P. G.: Flexible approach for quantifying average long-term changes and seasonal cycles of tropospheric trace species, Atmos. Meas. Tech., 12, 3383–3394, https://doi.org/10.5194/amt-12-3383-2019, 2019

Parrish, D. D., Derwent, R. G., Steinbrecht, W., Stübi, R., VanMalderen, R., Steinbacher, M., Trickl, T., Ries, L., and Xu, X.: Zonal similarity of long-term changes and seasonal cycles of baseline ozone at northern midlatitudes. J. Geophys. Res.: Atmos., doi: 10.1029/2019JD031908, 2020.

https://doi.org/10.5194/egusphere-2026-1939
Preprint. Discussion started: 10 April 2026
© Author(s) 2026. CC BY 4.0 License.

Parrish, D.D., Derwent, R.G., and Faloona, I.C.: Long-term baseline ozone changes in the Western US: A synthesis of analyses, Journal of the Air & Waste Management Association, DOI: 10.1080/10962247.2021.1945706, 2021a.

Parrish, D.D., Derwent, R.G., and Staehelin, J.: Long-term changes in northern mid-latitude tropospheric ozone concentrations: Synthesis of two recent analyses, Atmos. Environ., 248, https://doi.org/10.1016/j.atmosenv.2021.118227, 2021b.

Parrish, D. D., Derwent, R. G., Faloona, I. C., and Mims, C. A.: Technical note: Northern midlatitude baseline ozone – long-term changes and the COVID-19 impact, Atmos. Chem. Phys., 22, 13423–13430, https://doi.org/10.5194/acp-22-13423-2022, 2022.

Schnell, J. L., Prather, M. J., Josse, B., Naik, V., Horowitz, L. W., Zeng, G., Shindell, D. T., and Faluvegi, G.: Effect of climate change on surface ozone over North America, Europe, and East Asia. Geophysical research letters, 43(7), 3509–3518. https://doi.org/10.1002/2016GL068060, 2016.

Steinbrecht, W., Kubistin, D., Plass-Dülmer, C., Davies, J., Tarasick, D. W., v. d. Gathen, P., Deckelmann, H., Jepsen, N., Kivi, R., Lyall, N., Palm, M., Notholt, J., Kois, B., Oelsner, P., Allaart, M., Piters, A., Gill, M., Van Malderen, R., Delcloo, A. W., Sussmann, R., Mahieu, E., Servais, C., Romanens, G., Stübi, R., Ancellet, G., Godin-Beekmann, S., Yamanouchi, S., Strong, K., Johnson, B., Cullis, P., Petropavlovskikh, I., Hannigan, J. W., Hernandez, J.-L., Rodriguez, A. D., Nakano, T., Chouza, F., Leblanc, T., Torres, C., Garcia, O., Röhling, A. N., Schneider, M., Blumenstock, T., Tully, M., Paton-Walsh, C., Jones, N., Querel, R., Strahan, S., Stauffer, R. M., Thompson, A. M., Inness, A., Engelen, R., Chang, K.-L., and Cooper, O. R.: COVID–19 Crisis Reduces Free Tropospheric Ozone across the Northern Hemisphere, Geophys. Res. Lett., 48, e2020GL091987, https://doi.org/10.1029/2020GL091987, 2021.

Stevenson, D. S., Dentener, F. J., Schultz, M. G., Ellingsen, K., Van Noije, T. P. C., Wild, O., Zeng, G., Amann, M., Atherton, C. S., Bell, N., Bergmann, D. J., Bey, I., Butler, T., Cofala, J., Collins, W. J., Derwent, R. G., Doherty, R. M., Drevet, J., Eskes, H. J., Fiore, A. M., Gauss, M., Hauglustaine, D. A., Horowitz, L. W., Isaksen, I. S. A., Krol, M. C., Lamarque, J. -F., Lawrence, M. G., Montanaro, V., Müller, J. -F., Pitari, G., Prather, M. J., Pyle, J. A., Rast, S., Rodriguez, J. M., Sanderson, M. G., Savage, N. H., Shindell, D. T., Strahan, S. E., Sudo, K., and Szopa, S.: Multimodel ensemble simulations of present-day and near-future tropospheric ozone, J. Geophys. Res., 111, 2005JD006338, https://doi.org/10.1029/2005JD006338 , 2006.

Steinbrecht, W., Velazco, V. A., Dirksen, R., Doppler, L., Oelsner, P., Van Malderen, R., De Backer, H., Maillard Barras, E., Stübi, R., Godin-Beekmann, S., Hauchecorne, A.: Ground-based monitoring of stratospheric ozone and temperature over Germany since the 1960s. Earth and Space Science, 12, e2024EA003821. https://doi.org/10.1029/2024EA003821, 2025.

Tarasick, D., Galbally, I. E., Cooper, O. R., Schultz, M. G., Ancellet, G., Leblanc, T., Wallington, T. J., Ziemke, J., Liu, X., Steinbacher, M., Staehelin, J., Vigouroux, C., Hannigan, J. W., García, O., Foret, G., Zanis, P., Weatherhead, E., Petropavlovskikh, I., Worden, H., Osman, M., Liu, J., Chang, K.-L., Gaudel, A., Lin, M., Granados-Muñoz, M., Thompson, A. M., Oltmans, S. J., Cuesta, J., Dufour, G., Thouret, V., Hassler, B., Trickl, T., and Neu, J. L.: Tropospheric

https://doi.org/10.5194/egusphere-2026-1939
Preprint. Discussion started: 10 April 2026
© Author(s) 2026. CC BY 4.0 License.

ozone from 1877 to 2016, observed levels, trends and uncertainties, Elem. Sci. Anth., 7, 39, https://doi.org/10.1525/elementa.376, 2019.

Van Malderen, R., De Muer, D., De Backer, H., Poyraz, D., Verstraeten, W. W., De Bock, V., Delcloo, A. W., Mangold, A., Laffineur, Q., Allaart, M., Fierens, F. and Thouret. V.: Fifty years of balloon-borne ozone profile measurements at Uccle, Belgium: a short history, the scienti!c relevance, and the achievements in understanding the vertical ozone distribution. Atmos. Chem. Phys., 21, 12385–12411, https://doi.org/10.5194/acp-21-12385-2021, 2021.

Van Malderen, R., Thompson, A. M., Kollonige, D. E., Stau!er, R. M., Smit, H. G. J., Maillard Barras, E., Vigouroux, C., Petropavlovskikh, I., Leblanc, T., Thouret, V., Wol!, P., E!ertz, P., Tarasick, D. W., Poyraz, D., Ancellet, G., De Backer, M.-R., Evan, S., Flood, V., Frey, M. M., Hannigan, J. W., Hernandez, J. L., Iarlori, M., Johnson, B. J., Jones, N., Kivi, R., Mahieu, E., McConville, G., Müller, K., Nagahama, T., Notholt, J., Piters, A., Prats, N., Querel, R., Smale, D., Steinbrecht, W., Strong, K., and Sussmann, R.: Global groundbased tropospheric ozone measurements: reference data and individual site trends (2000–2022) from the TOAR-II/HEGIFTOM project, Atmos. Chem. Phys., 25, 7187–7225, https://doi.org/10.5194/acp-25-7187-2025, 2025.

Wild, O., and Palmer, P. I.: How sensitive is tropospheric oxidation to anthropogenic emissions?, Geophys. Res. Lett., 35, L22802, doi:10.1029/2008GL035718, 2008).

Young, P.J., Archibald, A. T., Bowman, K. W., Lamarque, J.-F., Naik, V., Stevenson, D. S., Tilmes, S., Voulgarakis, A., Wild, O., Bergmann, D., Cameron-Smith, P., Cionni, I., Collins, W. J., Dalsøren, S. B., Doherty, R. M., Eyring, V., Faluvegi, G., Horowitz, L. W., Josse, B., Lee, Y. H., MacKenzie, I. A., Nagashima, T., Plummer, D. A., Righi, M., Rumbold, S. T., Skeie, R. B., Shindell, D. T., Strode, S. A., Sudo, K., Szopa, S., and Zeng, G.: Pre-industrial to end 21st century projections of tropospheric ozone from the Atmospheric Chemistry and Climate Model Intercomparison Project (ACCMIP), Atmos. Chem. Phys., 13, 2063-2090, 2013.

Young, P. J., Naik, V., Fiore, A. M., Gaudel, A., Guo, J., Lin, M. Y., Neu, J. L., Parrish, D. D., Rieder, H. E., Schnell, J. L., Tilmes, S., Wild, O., Zhang, L., Ziemke, J., Brandt, J., Delcloo, A., Doherty, R. M., Geels, C., Hegglin, M. I., Hu, L., Im, U., Kumar, R., Luhar, A., Murray, L., Plummer, D., Rodriguez, J., Saiz-Lopez, A., Schultz, M. G., Woodhouse, M. T., and Zeng, G.: Tropospheric Ozone Assessment Report: Assessment of global-scale model performance for global and regional ozone distributions, variability, and trends. Elem Sci Anth, 6: 10. DOI: https://doi.org/10.1525/elementa.265, 2018.

Zhang, Y., Cooper, O. R., Gaudel, A., Thompson, A. M., Nédélec, P., Ogino, S.-Y., and West, J. J.: Tropospheric ozone change from 1980 to 2010 dominated by equatorward redistribution of emissions, Nat. Geosci., 9, 875–879, https://doi.org/10.1038/ngeo2827, 2016.